

A stabilised displacement–volumetric strain formulation for nearly incompressible and anisotropic materials

R. Rossi^{a,b,*}, R. Zorrilla^b, R. Codina^{a,b}

^a *Universitat Politècnica de Catalunya (UPC), Departament d'Enginyeria Civil i Ambiental, Spain*

^b *International Center for Numerical Methods in Engineering (CIMNE), Spain*

Received 23 July 2020; received in revised form 20 January 2021; accepted 24 January 2021

Available online 15 February 2021

Abstract

The simulation of structural problems involving the deformations of volumetric bodies is of paramount importance in many areas of engineering. Although the use of tetrahedral elements is extremely appealing, tetrahedral discretisations are generally known as very stiff and are hence often avoided in typical simulation workflows.

The development of mixed displacement–pressure approaches has allowed to effectively overcome this problem leading to a class of locking-free elements which can effectively compete with hexahedral discretisations while retaining obvious advantages in the mesh generation step. Despite such advantages the adoption of the technology within commercial codes is not yet pervasive.

This can be attributed to two different reasons: the difficulty in making use of standard constitutive libraries and the implied continuity of the pressure, which makes the application of the method questionable in the context of multi-material problems. Current paper proposes the adoption of the volumetric strain instead of the pressure as a nodal value. Such choice leads to the definition of a modified strain making the use of standard strain-driven constitutive laws straightforward. At the same time, the continuity of the volumetric strain across multimaterial interfaces can be understood as a sort of kinematic constraint (stresses can still remain discontinuous across material interfaces). The new element also opens the door to the use of anisotropic constitutive laws, which are typically problematic in the context of mixed elements.

© 2021 Elsevier B.V. All rights reserved.

Keywords: Finite elements; Mixed formulation; Anisotropic; Volumetric strain; Nearly incompressible materials; Variational multiscales

1. Motivation

The use of tetrahedral (or triangular) meshes in the simulation of complex geometries presents important advantages due to the availability of robust automatic mesh generation technologies. Unfortunately, tetrahedral meshes typically show poor accuracy and are very prone to locking when used in the vicinity of the incompressible limit. A number of proposals were developed over the years to retrofit such situation. One line of research, see e.g. [1,2], proposes the use of neighbourhood information to reconstruct an improved strain or displacement field. A different approach is based on the use of mixed formulations in which the displacement field is complemented

* Corresponding author at: Universitat Politècnica de Catalunya (UPC), Departament d'Enginyeria Civil i Ambiental, Spain.

E-mail addresses: rrossi@cimne.upc.edu (R. Rossi), rzorrilla@cimne.upc.edu (R. Zorrilla), ramon.codina@upc.edu (R. Codina).

by other variables. An early example in the context of structural mechanics can be found in [3], which proposes the use of a displacement–pressure–volumetric strain approach stabilised by the use of a bubble function for the displacement field. For such element the “bubble displacement” and volumetric strain (which is assumed to be only piece-wise continuous) can be statically condensed at the element level to provide a final form in terms of nodal displacements and pressures.

A more general framework to the development of stable, equal order, elements is provided by the Variational Multiscale Stabilisation which allows to sidestep the limitations of the inf–sup condition, known to be necessary and sufficient for the Galerkin method to be well posed. The development of stabilised, mixed Q_1/Q_1 (multi-linear/multi-linear) and P_1/P_1 (linear/linear) displacement–pressure approaches [4] has represented a milestone in the finite element (FE) technology, offering the possibility of improving the accuracy of low order meshes while guaranteeing a provably lock-free behaviour at the nearly-incompressible limit. The key idea of displacement–pressure ($\mathbf{u}-p$) approaches is to split the constitutive response into its deviatoric and volumetric parts. The deviatoric part of the strain is then recovered from the displacement field and introduced into the constitutive law, which returns the corresponding deviatoric stress. The volumetric part on the other hand is obtained in terms of the nodal pressure field. Even though this approach can effectively solve any volumetric locking issue, it implies that the total strain is never explicitly computed (in the FE implementation, only the deviatoric strain and pressure are available at the Gauss points). The practical downside of this issue is that one cannot make use of standard strain-driven constitutive laws. This represents a practical blocker in the context of commercial codes, which need to leverage large material libraries. The proposed approach overcomes such limitation by *choosing the volumetric strain ε^v , instead of the pressure, as primal variable*. In this way, the total strain can be recovered at the Gauss point level as the sum of the deviatoric part, obtained as before in terms of the displacement gradient, and the volumetric part, obtained by interpolating ε^v . Thus, the use of standard constitutive models becomes straightforward and the above described problem is effectively resolved.

The second well known difficulty, which is intrinsic to the use of equal-order mixed displacement–pressure fields, is that the pressure is treated as a continuous FE variable. This becomes problematic when multiple materials need to be considered within the domain, since in the presence of pressure discontinuities, continuous approximations typically manifest unwanted oscillations. Although this can be remedied for example by doubling the pressure degrees of freedom at the interface [5], such approach is normally inconvenient when more than two materials are present. On the contrary, the use of a continuous discretisation for ε^v does not impede the appearance of discontinuous pressures across the material interface, implying that this difficulty is effectively circumvented.

Interestingly, for isotropic linear constitutive relations the proposed formulation can be understood simply as a displacement–pressure approach with a change of variables. When considered in this context, the $\mathbf{u}-\varepsilon^v$ formulation inherits all the stability properties of the original $\mathbf{u}-p$ approach (see e.g. [6] for a recent discussion).

We shall also remark that the use of displacement–strain (total strain) formulations has been proposed in [7] as an alternative to the displacement–stress approach, also described in [7]. Moreover, an enhanced three field formulation (displacement–strain–pressure) $\mathbf{u}-\boldsymbol{\varepsilon}-p$ has recently been proposed in [8]. To the best of our knowledge however, this is the first time that a $\mathbf{u}-\varepsilon^v$ formulation is discussed in detail. To this end, the paper is structured as follows: a mixed displacement–volumetric strain formulation for small strain elasticity is derived as a special case of the displacement–strain formulation in Section 2, where the problem is set at the continuous level and an FE discretisation is proposed. The case of anisotropic materials is studied in Section 3, retrofitting the original formulation to allow the solution of anisotropic problems. This is accomplished by a redefinition of the modified volumetric strain which accounts for the anisotropic behaviour of the material. The article is concluded by a set of convergence tests in Section 4, that are performed for both the isotropic and anisotropic cases, as well as by a number of test examples assessing the performance of the proposed formulation. Finally, the last section collects the outcomes and further work lines of the paper.

The $\mathbf{u}-\varepsilon^v$ formulation that we propose is implemented within the open source [Kratos Multiphysics](#) framework [9,10].

2. Formulation

2.1. Governing equations

The essence of the proposed formulation is to modify the (small) strain definition to avoid volumetric locking. This is accomplished by employing a mixed formulation in which, the volumetric strain ε^v is considered as an

unknown, and interpolated as such when the problem is approximated using FE. The key idea is that the standard deviatoric–isochoric splitting is performed at the strain level. The deviatoric part is then computed in terms of the displacements while the isochoric one is expressed in terms of ε^v . This is expressed mathematically as

$$\boldsymbol{\varepsilon}(\mathbf{x}) = \underbrace{\nabla^s \mathbf{u} - \frac{1}{\alpha} \nabla \cdot \mathbf{u} \mathbf{I}}_{\boldsymbol{\varepsilon}_{\text{dev}}} + \underbrace{\frac{1}{\alpha} \varepsilon^v \mathbf{I}}_{\boldsymbol{\varepsilon}_{\text{iso}}} \quad (1)$$

where \mathbf{I} is the identity matrix. The coefficient α is taken here as $\alpha = 3$ in the 3D case and $\alpha = 2$ in the 2D one (both for plane strain and plane stress cases). This choice implies that in 2D plane stress cases, the “volumetric” strain should be understood as a measure of the area change in the plane rather than a measure of the real volume change.

Once the strain splitting is defined, the governing equations can be written as

$$-\nabla \cdot \boldsymbol{\sigma}(\boldsymbol{\varepsilon}) = \mathbf{f} \quad (2a)$$

$$\nabla \cdot \mathbf{u} - \varepsilon^v = 0 \quad (2b)$$

where the first equation is the classical equilibrium condition and the second one expresses the kinematic relation between the volume variation and the displacement field, which is exact for the small deformation case.

Up to this point, no assumption is made about the constitutive behaviour other than a dependency of the stress on the strain, $\boldsymbol{\sigma} = \boldsymbol{\sigma}(\boldsymbol{\varepsilon})$. More specifically, we remark that the formulation is not limited to the case of elastic materials and can include more complex models, which could eventually feature a dependency on internal variables (e.g. plasticity). Likewise, the introduction of the volumetric strain as a variable can be done both for stationary and time dependent problems, although in this paper we restrict ourselves to the former case.

Furthermore, we note that Eq. (2b) can be written in incremental form as

$$\nabla \cdot \Delta \mathbf{u} - \Delta \varepsilon^v = 0 \quad (3)$$

with $\Delta(\cdot)$ denoting an increment. In the case of linear problems, this choice is completely equivalent to Eq. (2b). However, it has some practical advantages in the application of initial conditions or the initial guess for iterative schemes.

2.2. Variational approach

Obtaining a symmetric variational form for the problem described in Eqs. (2a) and (2b) is not obvious. Our approach for doing so is to begin by considering the mixed displacement–strain form described in [7], or in [11,12] for the explicit case.

2.2.1. Standard \mathbf{u} - $\boldsymbol{\varepsilon}$ formulation

Let us start considering the differential form of the $\mathbf{u} - \boldsymbol{\varepsilon}$ formulation, which reads

$$-\nabla \cdot \mathbb{C} : \boldsymbol{\varepsilon} = \mathbf{f}$$

$$\mathbb{C} : \boldsymbol{\varepsilon} - \mathbb{C} : \nabla^s \mathbf{u} = \mathbf{0}$$

where \mathbb{C} is the constitutive tensor and \mathbf{f} denotes the vector of external body forces. To simplify the exposition, let us consider homogeneous Dirichlet boundary conditions $\mathbf{u} = \mathbf{0}$ on the whole boundary $\partial\Omega$ of the domain Ω where the problem is posed.

Let $\delta_{\mathbf{u}}$ (vanishing on the boundary) and $\delta_{\boldsymbol{\varepsilon}}$ be the displacement and strain test functions. The weak form of the problem consists of finding \mathbf{u} and $\boldsymbol{\varepsilon}$ in the appropriate spaces such that

$$\int_{\Omega} \nabla^s \delta_{\mathbf{u}} : \mathbb{C} : \boldsymbol{\varepsilon} = \int_{\Omega} \delta_{\mathbf{u}} \cdot \mathbf{f} \quad (4a)$$

$$-\int_{\Omega} \delta_{\boldsymbol{\varepsilon}} : \mathbb{C} : (\boldsymbol{\varepsilon} - \nabla^s \mathbf{u}) = 0 \quad (4b)$$

for all test functions $\delta_{\mathbf{u}}$ and $\delta_{\boldsymbol{\varepsilon}}$. The problem can also be written in the form

$$B_{\mathbf{u}\boldsymbol{\varepsilon}}(\mathbf{u}, \boldsymbol{\varepsilon}; \delta_{\mathbf{u}}, \delta_{\boldsymbol{\varepsilon}}) := \int_{\Omega} \nabla^s \delta_{\mathbf{u}} : \mathbb{C} : \boldsymbol{\varepsilon} - \int_{\Omega} \delta_{\boldsymbol{\varepsilon}} : \mathbb{C} : (\boldsymbol{\varepsilon} - \nabla^s \mathbf{u}) = \int_{\Omega} \delta_{\mathbf{u}} \cdot \mathbf{f} \quad (5)$$

It is observed that the bilinear form $B_{\mathbf{u}\boldsymbol{\varepsilon}}$ is semi-definite:

$$B_{\mathbf{u}\boldsymbol{\varepsilon}}(\mathbf{u}, \boldsymbol{\varepsilon}; \mathbf{u}, -\boldsymbol{\varepsilon}) = \int_{\Omega} \boldsymbol{\varepsilon} : \mathbb{C} : \boldsymbol{\varepsilon}$$

From this, one can easily get a stability estimate for the strain, but not for the displacement. An inf-sup condition is required to bound it in the continuous case, which needs to be inherited by the FE interpolation, unless a stabilised FE method is employed. A similar comment applies to the formulation that is to be proposed later.

If we introduce the functional

$$\mathcal{E}_{\mathbf{u}\boldsymbol{\varepsilon}}(\mathbf{u}, \boldsymbol{\varepsilon}) = \frac{1}{2} \int_{\Omega} (\boldsymbol{\varepsilon} - \nabla^s \mathbf{u}) : \mathbb{C} : (\boldsymbol{\varepsilon} - \nabla^s \mathbf{u}) - \frac{1}{2} \int_{\Omega} \nabla^s \mathbf{u} : \mathbb{C} : \nabla^s \mathbf{u} + \int_{\Omega} \mathbf{u} \cdot \mathbf{f}$$

it is easily seen that Eqs. (4) are precisely its stationary conditions. The way we have written $\mathcal{E}_{\mathbf{u}\boldsymbol{\varepsilon}}$ is intended to motivate the following formulation.

2.2.2. \mathbf{u} - ε^v Formulation

Our proposal is to start from the variational form of the \mathbf{u} - $\boldsymbol{\varepsilon}$ formulation and to substitute the strain formula $\boldsymbol{\varepsilon} := \nabla^s \mathbf{u} - \frac{1}{\alpha} \nabla \cdot \mathbf{u} \mathbf{I} + \frac{1}{\alpha} \varepsilon^v \mathbf{I}$ into it. Thus, let us consider the functional

$$\begin{aligned} \mathcal{E}_{\mathbf{u}\varepsilon^v}(\mathbf{u}, \varepsilon^v) &= \frac{1}{2} \frac{1}{\alpha^2} \int_{\Omega} (\varepsilon^v - \nabla \cdot \mathbf{u}) \mathbf{I} : \mathbb{C} : \mathbf{I} (\varepsilon^v - \nabla \cdot \mathbf{u}) \\ &\quad - \frac{1}{2} \int_{\Omega} \nabla^s \mathbf{u} : \mathbb{C} : \nabla^s \mathbf{u} + \int_{\Omega} \mathbf{u} \cdot \mathbf{f} \end{aligned} \tag{6}$$

Defining

$$\kappa := \frac{1}{\alpha^2} \mathbf{I} : \mathbb{C} : \mathbf{I} \tag{7}$$

which coincides with the volumetric modulus for isotropic materials, allows us to write the stationary conditions of the functional in Eq. (6) as

$$\begin{aligned} B_{\mathbf{u}\varepsilon^v}(\mathbf{u}, \varepsilon^v; \boldsymbol{\delta}_u, \delta_{\varepsilon^v}) &:= \int_{\Omega} (\delta_{\varepsilon^v} - \nabla \cdot \boldsymbol{\delta}_u) \kappa (\varepsilon^v - \nabla \cdot \mathbf{u}) \\ &\quad - \int_{\Omega} \nabla^s \boldsymbol{\delta}_u : \mathbb{C} : \nabla^s \mathbf{u} = - \int_{\Omega} \boldsymbol{\delta}_u \cdot \mathbf{f} \end{aligned} \tag{8}$$

for all test functions $\boldsymbol{\delta}_u, \delta_{\varepsilon^v}$. $B_{\mathbf{u}\varepsilon^v}$ is the counterpart of the bilinear form $B_{\mathbf{u}\boldsymbol{\varepsilon}}$ in Eq. (5) for the formulation we propose. The problem in Eq. (8) can also be split as

$$\int_{\Omega} \nabla^s \boldsymbol{\delta}_u : \mathbb{C} : \nabla^s \mathbf{u} + \int_{\Omega} \nabla \cdot \boldsymbol{\delta}_u \kappa (\varepsilon^v - \nabla \cdot \mathbf{u}) = \int_{\Omega} \boldsymbol{\delta}_u \cdot \mathbf{f} \tag{9a}$$

$$\int_{\Omega} \delta_{\varepsilon^v} \kappa (\varepsilon^v - \nabla \cdot \mathbf{u}) = 0 \tag{9b}$$

for all test functions $\boldsymbol{\delta}_u$ and δ_{ε^v} . This is the counterpart of Problem (4) obtained for the \mathbf{u} - ε^v formulation. The strong (differential) form of these equations (for a constant κ) is:

$$-\nabla \cdot \mathbb{C} : \nabla^s \mathbf{u} - \kappa \nabla (\varepsilon^v - \nabla \cdot \mathbf{u}) = \mathbf{f} \tag{10a}$$

$$\varepsilon^v - \nabla \cdot \mathbf{u} = 0 \tag{10b}$$

recalling that the zero Dirichlet conditions have been assumed throughout the boundary.

Remark 1. In the case of an arbitrary stress-strain relation, Problem (9) can be modified by replacing $\mathbb{C} : \nabla^s \mathbf{u}$ with the stress $\boldsymbol{\sigma}(\boldsymbol{\varepsilon})$ and introducing a scaling physical parameter $\tilde{\kappa}$ (with the same units as κ), so that the variational form of the problem would be

$$\int_{\Omega} \nabla^s \boldsymbol{\delta}_u : \boldsymbol{\sigma}(\boldsymbol{\varepsilon}) + \int_{\Omega} \nabla \cdot \boldsymbol{\delta}_u \tilde{\kappa} (\varepsilon^v - \nabla \cdot \mathbf{u}) = \int_{\Omega} \boldsymbol{\delta}_u \cdot \mathbf{f} \tag{11a}$$

$$\int_{\Omega} \delta_{\varepsilon^v} \tilde{\kappa} (\varepsilon^v - \nabla \cdot \mathbf{u}) = 0 \tag{11b}$$

for all test functions $\boldsymbol{\delta}_u$ and δ_{ε^v} . \square

Remark 2. Even though no assumption has been stated on \mathbb{C} to obtain Problem (9), we will use it only for isotropic materials; the way we deal with anisotropic cases is explained in Section 3. Consider then an isotropic material, and let us introduce Π_{dev} as the projection of second order tensors onto their deviatoric component. We may rewrite Eq. (10a) as

$$-\nabla \cdot \Pi_{\text{dev}}(\mathbb{C} : \nabla^s \mathbf{u}) - \frac{1}{\alpha} \nabla \cdot (\nabla \cdot \mathbf{u} \mathbb{C} : \mathbf{I}) - \kappa \nabla(\varepsilon^v - \nabla \cdot \mathbf{u}) = \mathbf{f} \tag{12}$$

For isotropic materials the property:

$$\frac{1}{\alpha} \nabla \cdot (\nabla \cdot \mathbf{u} \mathbb{C} : \mathbf{I}) = \kappa \nabla(\nabla \cdot \mathbf{u})$$

holds, hence Eq. (12) can be simplified to

$$-\nabla \cdot \Pi_{\text{dev}}(\mathbb{C} : \nabla^s \mathbf{u}) - \kappa \nabla \varepsilon^v = \mathbf{f}$$

The change of variable $p = \kappa \varepsilon^v$ yields the classical \mathbf{u} - p formulation of linear elasticity, which would allow us to deal with purely incompressible materials, i.e. $\kappa = \infty$. In this case, Eq. (10b) would be $\nabla \cdot \mathbf{u} = 0$. \square

Remark 3. In line with the previous remark, let us note that for anisotropic materials the incompressibility condition $\nabla \cdot \mathbf{u} = 0$ is *not* implied by any limiting value of a physical property as in the isotropic case, but by different conditions that relate the physical properties of an anisotropic material (see for example [13,14]). \square

2.3. Variational multi-scale stabilisation

Let us consider the continuous problem given in Eq. (8). The bilinear form of the problem satisfies

$$B_{\mathbf{u}\varepsilon^v}(\mathbf{u}, \varepsilon^v; -\mathbf{u}, \varepsilon^v) = \int_{\Omega} \kappa(\varepsilon^v)^2 - \int_{\Omega} \kappa(\nabla \cdot \mathbf{u})^2 + \int_{\Omega} \nabla^s \mathbf{u} : \mathbb{C} : \nabla^s \mathbf{u} \tag{13}$$

For isotropic materials, the second term is precisely the volumetric component of the third one, and since the deviatoric and volumetric components of a tensor are orthogonal, we are left with only the deviatoric part. In the case of anisotropic or nonlinear materials, the scaling coefficient $\tilde{\kappa}$ should be chosen such that the second term could be absorbed by the third one. In any case, it is observed that this expression provides control only over the deviatoric part of $\nabla^s \mathbf{u}$ and ε^v , that is to say, this expression will allow one to bound only the norm of these two functions, for which one will be able to obtain a stability estimate. Thus, we miss the control over the volumetric part of $\nabla^s \mathbf{u}$, which can be obtained at the continuous level from an inf-sup condition from the control over ε^v . This means that the norm of the volumetric part of $\nabla^s \mathbf{u}$ can be bounded in terms of the norm of ε^v provided the inf-sup condition holds. It is outside the scope of this paper to show how this can be done, but the procedure is similar to the bounding of the norm of the pressure from the bound on the norm of $\nabla^s \mathbf{u}$ and the inf-sup condition in the displacement-pressure formulation for incompressible materials. However, if we use the standard Galerkin FE discretisation, this inf-sup condition will not necessarily hold. Moreover, since derivatives of ε^v do not appear in Eq. (13), there is no guarantee to have them bounded, and the FE approximation to this variable may display node-to-node oscillations. This effect is particularly important in materials close to the incompressible limit, in which $\varepsilon^v \rightarrow 0$, even if $\kappa \rightarrow \infty$, $\kappa(\varepsilon^v)^2 \rightarrow 0$ (since $\kappa \varepsilon^v$ must remain bounded).

In our numerical experiments we have observed that the Galerkin approximation to the problem in Eq. (8) leads to severe node to node oscillations, similarly to what is found with other unstable mixed methods. In order to avoid such spurious oscillations, we now present a stabilised FE formulation based on the Variational Multi-Scale (VMS) concept [15,16].

Let us consider the domain Ω to be discretised in a partition $\{\Omega^e\}$ of elements with a characteristic size h and index e that ranges from 1 to the total number of elements. From this, we may construct the interpolating spaces for \mathbf{u} and ε^v ; standard continuous Lagrangian interpolations will be assumed for both variables. Henceforth, we will denote FE functions with the subscript h .

The VMS method is based on the separation of the unknown fields, in this case the displacement \mathbf{u} and the volumetric strain ε^v , in two scales. On one hand we have the scale which can be represented by the FE solution, \mathbf{u}_h and ε_h^v . On the other hand we have the so called sub-scales, which represent the part of the solution that cannot

be captured by the FE mesh and needs to be modelled. The sub-scales are denoted with the subindex s , as \mathbf{u}_s and ε_s^v . We thus have the decomposition

$$\mathbf{u} = \mathbf{u}_h + \mathbf{u}_s \tag{14a}$$

$$\varepsilon^v = \varepsilon_h^v + \varepsilon_s^v \tag{14b}$$

A similar splitting holds for the test functions, yielding an equation in the FE space as well as in the space of sub-scales. Here, the idea is to insert these splittings into the variational form of the problem, integrate by parts the terms involving derivatives of the sub-scales, and then, give an approximation for them (not for their derivatives).

Introducing the splitting presented in Eqs. (14) into Problem (9) and taking the test functions from the corresponding FE spaces, upon performing the integration by parts for each element, results in:

$$\begin{aligned} & \int_{\Omega} \nabla^s \delta_{\mathbf{u}_h} : \mathbb{C} : \nabla^s \mathbf{u}_h - \sum_e \int_{\Omega^e} \mathbf{u}_s \cdot \nabla \cdot \mathbb{C} : \nabla^s \delta_{\mathbf{u}_h} \\ & + \int_{\Omega} \nabla \cdot \delta_{\mathbf{u}_h} \kappa (\varepsilon_h^v + \varepsilon_s^v - \nabla \cdot \mathbf{u}_h) + \sum_e \int_{\Omega^e} \mathbf{u}_s \cdot \kappa \nabla \nabla \cdot \delta_{\mathbf{u}_h} \\ & = \int_{\Omega} \delta_{\mathbf{u}_h} \cdot \mathbf{f} \end{aligned} \tag{15a}$$

$$\int_{\Omega} \delta_{\varepsilon_h^v} \kappa (\varepsilon_h^v + \varepsilon_s^v - \nabla \cdot \mathbf{u}_h) + \sum_e \int_{\Omega^e} \mathbf{u}_s \cdot \kappa \nabla \delta_{\varepsilon_h^v} = 0 \tag{15b}$$

where the sub-scales have been discarded on the element boundaries, although this assumption can be relaxed as it is described in [17]. Combining Eqs. (15) we have:

$$\begin{aligned} & \int_{\Omega} \nabla^s \delta_{\mathbf{u}_h} : \mathbb{C} : \nabla^s \mathbf{u}_h + \int_{\Omega} (\delta_{\varepsilon_h^v} + \nabla \cdot \delta_{\mathbf{u}_h}) \kappa (\varepsilon_h^v - \nabla \cdot \mathbf{u}_h) \\ & + \sum_e \int_{\Omega^e} \mathbf{u}_s \cdot [-\nabla \cdot \mathbb{C} : \nabla^s \delta_{\mathbf{u}_h} + \kappa \nabla (\varepsilon_h^v + \nabla \cdot \delta_{\mathbf{u}_h})] \\ & + \sum_e \int_{\Omega^e} \varepsilon_s^v \kappa (\delta_{\varepsilon_h^v} + \nabla \cdot \delta_{\mathbf{u}_h}) = \int_{\Omega} \delta_{\mathbf{u}_h} \cdot \mathbf{f} \end{aligned} \tag{16}$$

The model is completed by choosing an approximation for the sub-scales. The counterpart of Eq. (16) with the test functions taken from the space of sub-scales would lead to an equation projected onto this space, stating that the differential operator of the problem is equal to the residual of the FE scales. This operator applied to the sub-scales can then be approximated by a diagonal matrix using different arguments (see [16] for a review and details). In view of the equations to be solved (10), the final result is

$$\mathbf{u}_s = \tau_1 P_s [\mathbf{f} + \nabla \cdot \mathbb{C} : \nabla^s \mathbf{u}_h + \kappa \nabla (\varepsilon_h^v - \nabla \cdot \mathbf{u}_h)] \tag{17a}$$

$$\varepsilon_s^v = \tau_2 P_s [\nabla \cdot \mathbf{u}_h - \varepsilon_h^v] \tag{17b}$$

where τ_1 and τ_2 are the stabilisation parameters, given below, and P_s is the projection onto the space of sub-scales, of either \mathbf{u}_s or ε_s^v .

Inserting the sub-scales given by Eqs. (17) into Eq. (16), we finally obtain the stabilised FE method we propose, which consists in finding \mathbf{u}_h and ε_h^v such that

$$\begin{aligned} & B_{\mathbf{u}\varepsilon^v, \text{stab}}(\mathbf{u}_h, \varepsilon_h^v; \delta_{\mathbf{u}_h}, \delta_{\varepsilon_h^v}) \\ & := \int_{\Omega} \nabla^s \delta_{\mathbf{u}_h} : \mathbb{C} : \nabla^s \mathbf{u}_h + \int_{\Omega} (\delta_{\varepsilon_h^v} + \nabla \cdot \delta_{\mathbf{u}_h}) \kappa (\varepsilon_h^v - \nabla \cdot \mathbf{u}_h) \\ & + \sum_e \int_{\Omega^e} \tau_1 P_s [\nabla \cdot \mathbb{C} : \nabla^s \mathbf{u}_h + \kappa \nabla (\varepsilon_h^v - \nabla \cdot \mathbf{u}_h)] \\ & \quad \cdot [-\nabla \cdot \mathbb{C} : \nabla^s \delta_{\mathbf{u}_h} + \kappa \nabla (\delta_{\varepsilon_h^v} + \nabla \cdot \delta_{\mathbf{u}_h})] \\ & + \sum_e \int_{\Omega^e} \tau_2 P_s (\nabla \cdot \mathbf{u}_h - \varepsilon_h^v) \kappa (\delta_{\varepsilon_h^v} + \nabla \cdot \delta_{\mathbf{u}_h}) \end{aligned}$$

$$\begin{aligned}
 &= \int_{\Omega} \delta_{\mathbf{u}_h} \cdot \mathbf{f} - \sum_e \int_{\Omega^e} \tau_1 P_s[\mathbf{f}] \cdot [-\nabla \cdot \mathbb{C} : \nabla^s \delta_{\mathbf{u}_h} + \kappa \nabla(\delta_{\varepsilon_h^v} + \nabla \cdot \delta_{\mathbf{u}_h})] \\
 &:= L_{\mathbf{u}^v, \text{stab}}(\delta_{\mathbf{u}_h}, \delta_{\varepsilon_h^v})
 \end{aligned} \tag{18}$$

for all test functions $\delta_{\mathbf{u}_h}$ and $\delta_{\varepsilon_h^v}$.

To complete the definition of the method, we need to define the projection P_s and the expression of the stabilisation parameters. Even though the space for the sub-scales can be defined in different manners (bubble functions, approximation to Green’s function, etc.), when arriving at Eq. (17) there are essentially two options, namely, to take the space of sub-scale as the space of FE residuals, yielding $P_s = I$ (the identity) or to take it as L^2 orthogonal to the FE space, case in which P_s is the orthogonal projection to this space. The second option has theoretical and practical advantages, as reported for example in [7,18–20]. However, here we will consider the most common option of taking $P_s = I$, which leads to classical residual-based stabilised FE methods. See also [16] for further discussion.

Regarding the stabilisation parameters, they can be determined by scaling arguments or by assuming that the sub-scales are bubble functions. In either case, the result is that they should behave as

$$\tau_1 = c_1 \frac{h^2}{G}, \quad \tau_2 = c_2 \frac{G}{G + \kappa} \tag{19}$$

where G is an equivalent effective shear modulus, and c_1 and c_2 are algorithmic constants, which we take as $c_1 = 2$, $c_2 = 4$ for triangles and tetrahedra. Let us remark that the definition of an “equivalent effective shear modulus” is not univocal in the context of anisotropic materials. We defer the discussion on the exact definition of such term to the following sections.

The formulation we propose is given by Eq. (18) with $P_s = I$ in combination with the τ_1 and τ_2 values given in Eq. (19). Considering the case of linear elements, in which second derivatives inside the elements are zero, Eq. (18) can be arranged to give

$$\begin{aligned}
 &B_{\mathbf{u}^v, \text{stab}, \text{lin}}(\mathbf{u}_h, \varepsilon_h^v; \delta_{\mathbf{u}_h}, \delta_{\varepsilon_h^v}) \\
 &:= \int_{\Omega} \nabla^s \delta_{\mathbf{u}_h} : \mathbb{C} : \nabla^s \mathbf{u}_h + \int_{\Omega} (1 - \tau_2)(\delta_{\varepsilon_h^v} + \nabla \cdot \delta_{\mathbf{u}_h}) \kappa (\varepsilon_h^v - \nabla \cdot \mathbf{u}_h) \\
 &\quad + \int_{\Omega} \tau_1 \kappa^2 \nabla \delta_{\varepsilon_h^v} \cdot \nabla \varepsilon_h^v = \int_{\Omega} \delta_{\mathbf{u}_h} \cdot \mathbf{f} - \int_{\Omega} \tau_1 \mathbf{f} \cdot \kappa \nabla \delta_{\varepsilon_h^v}
 \end{aligned} \tag{20}$$

Remark 4. Even though it is not the purpose of this paper to analyse the stability and convergence properties of the method in detail, the simplified problem presented in Eq. (20) allows us to understand the effect of τ_1 and τ_2 on the stability. Assuming both τ_1 and τ_2 to be constant for the sake of simplicity, we have that

$$\begin{aligned}
 B_{\mathbf{u}^v, \text{stab}, \text{lin}}(\mathbf{u}_h, \varepsilon_h^v; \mathbf{u}_h, \varepsilon_h^v) &= \|\mathbb{C}^{1/2} : \nabla^s \mathbf{u}_h\|^2 + (1 - \tau_2) \|\kappa^{1/2} \varepsilon_h^v\|^2 \\
 &\quad - (1 - \tau_2) \|\kappa^{1/2} \nabla \cdot \mathbf{u}_h\|^2 + \tau_1 \|\kappa \nabla \delta_{\varepsilon_h^v}\|^2
 \end{aligned}$$

where $\mathbb{C}^{1/2}$ is the square root of the positive-definite tensor \mathbb{C} and $\|\cdot\|$ is the L^2 norm in Ω . From this expression we observe that

- τ_2 reduces the (positive) L^2 control on ε_h^v .
- τ_2 reduces the subtracting L^2 norm of $\nabla \cdot \mathbf{u}_h$.
- τ_1 provides control on the derivatives of ε_h^v .

It is observed that the crucial parameter from the numerical point of view is τ_1 and that we need to ensure that $\tau_2 < 1$. \square

Remark 5. In order to be able to use generic materials we may proceed as indicated in Remark 1. If $\tilde{\kappa}$ is an adequate physical scaling parameter, the problem to be solved for a general constitutive law $\boldsymbol{\sigma} = \boldsymbol{\sigma}(\boldsymbol{\varepsilon})$ is

$$\begin{aligned}
 &\int_{\Omega} \nabla^s \delta_{\mathbf{u}_h} : \boldsymbol{\sigma}(\boldsymbol{\varepsilon}_h) + \int_{\Omega} (1 - \tau_2)(\delta_{\varepsilon_h^v} + \nabla \cdot \delta_{\mathbf{u}_h}) \tilde{\kappa} (\varepsilon_h^v - \nabla \cdot \mathbf{u}_h) \\
 &\quad + \int_{\Omega} \tau_1 \tilde{\kappa}^2 \nabla \delta_{\varepsilon_h^v} \cdot \nabla \varepsilon_h^v = \int_{\Omega} \delta_{\mathbf{u}_h} \cdot \mathbf{f} - \int_{\Omega} \tau_1 \mathbf{f} \cdot \tilde{\kappa} \nabla \delta_{\varepsilon_h^v}
 \end{aligned} \tag{21}$$

We remark here that the stabilisation factor τ_2 does not enter in the definition of the FE strain $\boldsymbol{\varepsilon}_h$, and is hence not employed in the calculation of the stress.

The formulation given by Eq. (21) reduces to the linear one when the strain $\boldsymbol{\varepsilon}_h = \nabla^s \mathbf{u}_h$ is used in the constitutive law. Another choice is to include the ε_h^v in the $\boldsymbol{\varepsilon}_h$ calculation. This choice, which comes from the (admittedly heuristic) rationale that such enhanced strain is “better” at the Gauss point level, leads to the modified strain

$$\boldsymbol{\varepsilon}_h := \nabla^s \mathbf{u}_h - \frac{1}{\alpha} \nabla \cdot \mathbf{u}_h \mathbf{I} + \frac{1}{\alpha} \varepsilon_h^v \mathbf{I} \tag{22}$$

Should this be the case, the first term on the left hand side of Eq. (21) becomes

$$\int_{\Omega} \nabla^s \delta \mathbf{u}_h : \left[\boldsymbol{\sigma}(\boldsymbol{\varepsilon}_h) - \mathbb{C} : \left(-\frac{1}{\alpha} \nabla \cdot \mathbf{u}_h \mathbf{I} + \frac{1}{\alpha} \varepsilon_h^v \mathbf{I} \right) \right] \tag{23}$$

where $\mathbb{C} := \left. \frac{\partial \boldsymbol{\sigma}}{\partial \boldsymbol{\varepsilon}_h} \right|_{\boldsymbol{\varepsilon}_h}$ should be interpreted as the tangent constitutive tensor of the constitutive law.

As we will show later, the tangent matrix of a Newton–Raphson linearisation of the problem described in Eq. (21), which assumes $\boldsymbol{\varepsilon}_h = \nabla^s \mathbf{u}_h$, is identical to that one obtained after inserting the modification in Eq. (23), which includes the modified strain given by Eq. (22). In any case, we note that the residual would of course be different. In our numerical examples, we have employed the modification in Eq. (23), although similar results are expected if such modification is not considered. \square

2.4. Finite element implementation—Isotropic case

A number of, rather standard, definitions are useful to write the FE discretisation of the proposed discrete variational problem (Eq. (21)). For a node I of the FE mesh, let N_I be its standard (Lagrangian) shape function while x, y, z denote its Cartesian coordinates. Furthermore, let us introduce the following arrays, whose definition depends on the number of space dimensions

$$\mathbf{B}_I = \begin{pmatrix} \frac{\partial N_I}{\partial x} & 0 & 0 \\ 0 & \frac{\partial N_I}{\partial y} & 0 \\ 0 & 0 & \frac{\partial N_I}{\partial z} \\ \frac{\partial N_I}{\partial y} & \frac{\partial N_I}{\partial x} & 0 \\ 0 & \frac{\partial N_I}{\partial z} & \frac{\partial N_I}{\partial y} \\ \frac{\partial N_I}{\partial z} & 0 & \frac{\partial N_I}{\partial x} \end{pmatrix} \text{ (3D) , } \mathbf{B}_I = \begin{pmatrix} \frac{\partial N_I}{\partial x} & 0 \\ 0 & \frac{\partial N_I}{\partial y} \\ \frac{\partial N_I}{\partial y} & \frac{\partial N_I}{\partial x} \end{pmatrix} \text{ (2D)} \tag{24}$$

$$\mathbf{m} := \begin{pmatrix} 1 \\ 1 \\ 1 \\ 0 \\ 0 \\ 0 \end{pmatrix} \text{ (3D) , } \mathbf{m} := \begin{pmatrix} 1 \\ 1 \\ 0 \end{pmatrix} \text{ (2D)} \tag{25}$$

$$\mathbf{G}_I := \begin{pmatrix} \frac{\partial N_I}{\partial x} \\ \frac{\partial N_I}{\partial y} \\ \frac{\partial N_I}{\partial z} \end{pmatrix} \text{ (3D) , } \mathbf{G}_I := \begin{pmatrix} \frac{\partial N_I}{\partial x} \\ \frac{\partial N_I}{\partial y} \end{pmatrix} \text{ (2D)} \tag{26}$$

$$\mathbf{P} := \mathbf{I} - \frac{1}{\alpha} \mathbf{m} \mathbf{m}^t \tag{27}$$

$$\kappa := \frac{\mathbf{m}^t \mathbf{C} \mathbf{m}}{\alpha^2} \tag{28}$$

where \mathbf{C} is the Voigt representation of the tangent constitutive tensor $\mathbb{C} := \left. \frac{\partial \boldsymbol{\sigma}}{\partial \boldsymbol{\varepsilon}_h} \right|_{\boldsymbol{\varepsilon}_h}$.

The FE residual varies slightly depending on the choice of $\boldsymbol{\varepsilon}_h$ (see Remark 5). If we choose $\boldsymbol{\varepsilon}_h := \nabla^s \mathbf{u}_h - \frac{1}{\alpha} \nabla \cdot \mathbf{u}_h \mathbf{I} + \frac{1}{\alpha} \boldsymbol{\varepsilon}_h^v \mathbf{I}$ (option we followed in our implementation) the residual is

$$\mathbf{R}_I := \left(N_I \mathbf{f} - \mathbf{B}_I^t \boldsymbol{\sigma}(\boldsymbol{\varepsilon}_h) + \frac{1}{\alpha} \mathbf{B}_I^t \mathbf{C} \mathbf{m} (N_J \boldsymbol{\varepsilon}_{h,J}^v - \mathbf{G}_J^t \mathbf{u}_{h,J}) - (1 - \tau_2) \kappa \mathbf{G}_I (N_J \boldsymbol{\varepsilon}_{h,J}^v - \mathbf{G}_J^t \mathbf{u}_{h,J}) \right) \\ (1 - \tau_2) \kappa N_I (N_J \boldsymbol{\varepsilon}_{h,J}^v - \mathbf{G}_J^t \mathbf{u}_{h,J}) + \kappa^2 \mathbf{G}_I^t \tau_1 \mathbf{G}_J \boldsymbol{\varepsilon}_{h,J}^v - \kappa \mathbf{G}_I^t \tau_1 \mathbf{f} \quad (29)$$

and if $\boldsymbol{\varepsilon}_h := \nabla^s \mathbf{u}_h$ is chosen, the residual simplifies to

$$\mathbf{R}_I := \left(N_I \mathbf{f} - \mathbf{B}_I^t \boldsymbol{\sigma}(\boldsymbol{\varepsilon}_h) - (1 - \tau_2) \kappa \mathbf{G}_I (N_J \boldsymbol{\varepsilon}_{h,J}^v - \mathbf{G}_J^t \mathbf{u}_{h,J}) \right) \\ (1 - \tau_2) \kappa N_I (N_J \boldsymbol{\varepsilon}_{h,J}^v - \mathbf{G}_J^t \mathbf{u}_{h,J}) + \kappa^2 \mathbf{G}_I^t \tau_1 \mathbf{G}_J \boldsymbol{\varepsilon}_{h,J}^v - \kappa \mathbf{G}_I^t \tau_1 \mathbf{f} \quad (30)$$

The definition of the discrete problem is completed by the Newton–Raphson linearisation. The derivative of the stress term can be computed as

$$\mathbf{B}_I^t \frac{\partial \boldsymbol{\sigma}(\boldsymbol{\varepsilon})}{\partial \mathbf{u}_{h,J}} = \mathbf{B}_I^t \frac{\partial \boldsymbol{\sigma}(\boldsymbol{\varepsilon})}{\partial \boldsymbol{\varepsilon}} \frac{\partial \boldsymbol{\varepsilon}}{\partial \mathbf{u}_{h,J}} = \mathbf{B}_I^t \frac{\partial \boldsymbol{\sigma}(\boldsymbol{\varepsilon})}{\partial \boldsymbol{\varepsilon}} \frac{\partial (\nabla^s \mathbf{u}_h - \frac{1}{\alpha} \nabla \cdot \mathbf{u}_h \mathbf{I} + \frac{1}{\alpha} \boldsymbol{\varepsilon}_h^v \mathbf{I})}{\partial \mathbf{u}_{h,J}} \\ = \mathbf{B}_I^t \mathbf{C} \mathbf{B}_J - \frac{1}{\alpha} \mathbf{B}_I^t \mathbf{C} \mathbf{m} \mathbf{G}_J^t \quad (31)$$

and

$$\mathbf{B}_I^t \frac{\partial \boldsymbol{\sigma}(\boldsymbol{\varepsilon})}{\partial \boldsymbol{\varepsilon}_h^v} = \mathbf{B}_I^t \frac{\partial \boldsymbol{\sigma}(\boldsymbol{\varepsilon})}{\partial \boldsymbol{\varepsilon}} \frac{\partial \boldsymbol{\varepsilon}}{\partial \boldsymbol{\varepsilon}_h^v} = \mathbf{B}_I^t \frac{\partial \boldsymbol{\sigma}(\boldsymbol{\varepsilon})}{\partial \boldsymbol{\varepsilon}} \frac{\partial (\nabla^s \mathbf{u}_h - \frac{1}{\alpha} \nabla \cdot \mathbf{u}_h \mathbf{I} + \frac{1}{\alpha} \boldsymbol{\varepsilon}_h^v \mathbf{I})}{\partial \boldsymbol{\varepsilon}_h^v} \\ = \frac{1}{\alpha} \mathbf{B}_I^t \mathbf{C} \mathbf{m} N_J \quad (32)$$

This allows to obtain the tangent operator as

$$\text{LHS}_{IJ} := \begin{pmatrix} \mathbf{B}_I^t \mathbf{C} \mathbf{B}_J - (1 - \tau_2) \kappa \mathbf{G}_I \mathbf{G}_J^t & (1 - \tau_2) \kappa \mathbf{G}_I N_J \\ (1 - \tau_2) \kappa N_I \mathbf{G}_J^t & - (1 - \tau_2) \kappa N_I N_J - \tau_1 \kappa^2 \mathbf{G}_I^t \mathbf{G}_J \end{pmatrix} \quad (33)$$

providing as expected a symmetric tangent (provided that \mathbf{C} is symmetric).

Remark 6. Note that the same expression of the tangent matrix is obtained independently on the definition of $\boldsymbol{\varepsilon}_h$. We observe however that for a non linear material, the current value of the constitutive tensor, which we recall is defined as $\mathbb{C} := \left. \frac{\partial \boldsymbol{\sigma}}{\partial \boldsymbol{\varepsilon}_h} \right|_{\boldsymbol{\varepsilon}_h}$, may vary according to the previous definition of $\boldsymbol{\varepsilon}_h$, and thus result in a different stiffness matrix. \square

3. Anisotropy

The proposed formulation works properly when the material is approximately isotropic; however, experimentation with strongly anisotropic materials shows that instabilities appear in both the volumetric strain and the displacement fields. A possibility to address this problem is to reduce the anisotropic case to a “similar” isotropic problem, for which the method is known to perform well. To this end, we observe that any anisotropic tensor \mathbb{C} can be written as $\mathbb{C} = \mathbb{T}^t : \hat{\mathbb{C}} : \mathbb{T}$ where $\hat{\mathbb{C}}$ is an *isotropic* elasticity tensor. Such property will allow us to propose a slight change in the choice of our modified volumetric strain. The following subsections detail first the construction of the “isotropic mapping” and to then introduce the proposed change in the definition of the volumetric strain.

3.1. Constitutive tensor scaling: the closest isotropic tensor

The property $\mathbb{C} = \mathbb{T}^t : \hat{\mathbb{C}} : \mathbb{T}$ is easily proved by construction. Let us assume that \mathbf{C} and $\hat{\mathbf{C}}$ are the Voigt counterparts of \mathbb{C} and $\hat{\mathbb{C}}$, which are known to be symmetric and positive definite and hence admit a square root. Thus, by defining $\mathbf{c} := \mathbf{C}^{1/2}$ and $\hat{\mathbf{c}} := \hat{\mathbf{C}}^{1/2}$, and considering that these matrices are also symmetric, we can write

$$\mathbf{C} = \mathbf{c} \mathbf{c} = \mathbf{c}^t \mathbf{c} = \mathbf{T}^t \hat{\mathbf{C}} \mathbf{T} = \mathbf{T}^t \hat{\mathbf{c}}^t \hat{\mathbf{c}} \mathbf{T} \quad (34)$$

which implies that

$$\mathbf{c} = \hat{\mathbf{c}} \mathbf{T} \implies \mathbf{T} = \hat{\mathbf{c}}^{-1} \mathbf{c} \quad (35)$$

Even though such decomposition is valid for any choice of $\hat{\mathbf{C}}$, in practice it is convenient to choose such tensor as close as possible to its anisotropic counterpart in order to guarantee that for an initially isotropic material the matrix \mathbf{T} is exactly the identity. Following the ideas presented in [21], we choose the $\hat{\mathbf{C}}$ tensor that minimises the Frobenius norm $\|\mathbf{C} - \hat{\mathbf{C}}\|_F$, with the additional constraint of exactly representing the bulk modulus of the original anisotropic tensor (Eq. (7)). This gives rise to the formulas

$$\hat{\mathbf{C}} = 3 \left(\frac{\alpha}{3} \kappa \right) \mathbf{J} + 2\mu \mathbf{K} \tag{36}$$

where $\mathbf{J} := \mathbf{t}\mathbf{t}^t$ and $\mathbf{K} := \mathbf{I}_4 - \mathbf{J}$, with \mathbf{t} defined as

$$\mathbf{t} := \begin{pmatrix} \frac{1}{\sqrt{3}} \\ \frac{1}{\sqrt{3}} \\ \frac{1}{\sqrt{3}} \\ 0 \\ 0 \\ 0 \end{pmatrix} (3D), \quad \mathbf{t} := \begin{pmatrix} \frac{1}{\sqrt{2}} \\ \frac{1}{\sqrt{2}} \\ 0 \end{pmatrix} (2D) \tag{37}$$

and

$$\mathbf{I}_4 = \begin{pmatrix} 1 & 0 & 0 & 0 & 0 & 0 \\ 0 & 1 & 0 & 0 & 0 & 0 \\ 0 & 0 & 1 & 0 & 0 & 0 \\ 0 & 0 & 0 & 0.5 & 0 & 0 \\ 0 & 0 & 0 & 0 & 0.5 & 0 \\ 0 & 0 & 0 & 0 & 0 & 0.5 \end{pmatrix} (3D), \quad \mathbf{I}_4 = \begin{pmatrix} 1 & 0 & 0 \\ 0 & 1 & 0 \\ 0 & 0 & 0.5 \end{pmatrix} (2D) \tag{38}$$

Using Voigt’s notation, the bulk modulus κ defined in Eq. (7) and appearing in Eq. (36) is

$$\kappa = \frac{\mathbf{m}^t \mathbf{C} \mathbf{m}}{\alpha^2} \tag{39}$$

which enforces that the bulk of the original anisotropic tensor \mathbf{C} coincides exactly with that of the “closest” tensor $\hat{\mathbf{C}}$.

Under these assumptions, the 1st Lamé parameter μ of the closest isotropic tensor in Eq. (36) can be obtained in closed form by minimising the Frobenius error norm $\|\mathbf{C} - \hat{\mathbf{C}}\|_F$ to give

$$\mu = 0.2(C_{00} - 2C_{01} + C_{11} + C_{22}) (2D) \tag{40a}$$

$$\begin{aligned} \mu = \frac{4}{33} [C_{00} - C_{01} - C_{02} + C_{11} - C_{12} + C_{22} \\ + \frac{3}{4}(C_{33} + C_{44} + C_{55})] (3D) \end{aligned} \tag{40b}$$

3.2. Variational approach

With the proposed mapping, the mixed strain–displacement problem presented in Eq. (4) becomes

$$\int_{\Omega} \nabla^s \delta_{\mathbf{u}} : \mathbb{T}^t : \hat{\mathbf{C}} : \mathbb{T} : \boldsymbol{\varepsilon} = \int_{\Omega} \delta_{\mathbf{u}} \cdot \mathbf{f} \tag{41a}$$

$$- \int_{\Omega} \delta_{\boldsymbol{\varepsilon}} : \mathbb{T}^t : \hat{\mathbf{C}} : \mathbb{T} : (\boldsymbol{\varepsilon} - \nabla^s \mathbf{u}) = 0 \tag{41b}$$

which shows an obvious similarity to the isotropic case once we define $\hat{\boldsymbol{\varepsilon}} := \mathbb{T} : \boldsymbol{\varepsilon}$ (and likewise for the test function). The essential idea of our proposal is hence to modify $\hat{\boldsymbol{\varepsilon}}$ instead of $\boldsymbol{\varepsilon}$ to obtain an equation in terms of the volumetric strain. Doing so we obtain

$$\hat{\boldsymbol{\varepsilon}} = \mathbb{T} : \nabla^s \mathbf{u} - \frac{1}{\alpha} \text{Tr}(\mathbb{T} : \nabla^s \mathbf{u}) \mathbf{I} + \frac{1}{\alpha} \varepsilon^v \mathbf{I}$$

What follows is simply an algebraic exercise to follow the same steps as in the general case, now particularised to the proposed change of variables.

Taking into account that $\mathbb{T}^{-1} : \mathbb{T} = \mathbb{T} : \mathbb{T}^{-1} = \mathbb{I}$ and that the trace can be written as $\text{Tr}(\mathbb{T} : \nabla^s \mathbf{u}) = \mathbf{I} : \mathbb{T} : \nabla^s \mathbf{u}$, we obtain

$$\hat{\boldsymbol{\varepsilon}} = \mathbb{T} : \nabla^s \mathbf{u} - \frac{\mathbf{I} : \mathbb{T} : \nabla^s \mathbf{u}}{\alpha} \mathbb{T} : \mathbb{T}^{-1} : \mathbf{I} + \frac{\hat{\varepsilon}^v}{\alpha} \mathbb{T} : \mathbb{T}^{-1} : \mathbf{I} \quad (42)$$

Premultiplying by \mathbb{T}^{-1} we can recover the enrichment of the original strain as

$$\boldsymbol{\varepsilon} = \nabla^s \mathbf{u} - \frac{\mathbf{I} : \mathbb{T} : \nabla^s \mathbf{u}}{\alpha} \mathbb{T}^{-1} : \mathbf{I} + \frac{\hat{\varepsilon}^v}{\alpha} \mathbb{T}^{-1} : \mathbf{I} \quad (43)$$

Note that for isotropic materials with $\mathbb{T} = \mathbb{I}$ the original formulation is recovered.

Once arrived at this point, the derivation follows exactly the same path as in the general case. By substituting Eq. (42) into Eqs. (41a) and (41b) we obtain

$$\int_{\Omega} \nabla^s \boldsymbol{\delta}_u : \mathbb{T}^t : \hat{\mathbb{C}} : \left(\mathbb{T} : \nabla^s \mathbf{u} - \frac{\mathbf{I} : \mathbb{T} : \nabla^s \mathbf{u}}{\alpha} \mathbf{I} + \frac{\hat{\varepsilon}^v}{\alpha} \mathbf{I} \right) = \int_{\Omega} \boldsymbol{\delta}_u \cdot \mathbf{f}$$

and by proceeding similarly for the strain test function we have

$$- \int_{\Omega} \left(\nabla^s \boldsymbol{\delta}_u : \mathbb{T}^t - \frac{\mathbf{I} : \mathbb{T} : \nabla^s \boldsymbol{\delta}_u}{\alpha} \mathbf{I} + \frac{\delta_{\hat{\varepsilon}^v}}{\alpha} \mathbf{I} \right) : \hat{\mathbb{C}} : \left(- \frac{\mathbf{I} : \mathbb{T} : \nabla^s \mathbf{u}}{\alpha} \mathbf{I} + \frac{\hat{\varepsilon}^v}{\alpha} \mathbf{I} \right) = 0$$

Substituting $\mathbb{T}^t : \hat{\mathbb{C}} : \mathbb{T}$ by the original \mathbb{C} and then rearranging and collecting the relevant terms leads to

$$\begin{aligned} & \int_{\Omega} \nabla^s \boldsymbol{\delta}_u : \mathbb{C} : \nabla^s \mathbf{u} \\ & - \int_{\Omega} \left(- \frac{\mathbf{I} : \mathbb{T} : \nabla^s \boldsymbol{\delta}_u}{\alpha} \right) \mathbf{I} : \mathbb{T}^{-t} : \mathbb{C} : \mathbb{T}^{-1} : \mathbf{I} \left(- \frac{\mathbf{I} : \mathbb{T} : \nabla^s \mathbf{u}}{\alpha} + \frac{\hat{\varepsilon}^v}{\alpha} \right) \\ & = \int_{\Omega} \boldsymbol{\delta}_u \cdot \mathbf{f} \end{aligned} \quad (44a)$$

$$- \int_{\Omega} \left(\frac{\delta_{\hat{\varepsilon}^v}}{\alpha} \right) \mathbf{I} : \mathbb{T}^{-t} : \mathbb{C} : \mathbb{T}^{-1} : \mathbf{I} \left(- \frac{\mathbf{I} : \mathbb{T} : \nabla^s \mathbf{u}}{\alpha} + \frac{\hat{\varepsilon}^v}{\alpha} \right) = 0 \quad (44b)$$

Unfortunately, the previous form is not fully convenient for modelling the mechanical response as the constitutive law input strain would be $\nabla^s \mathbf{u}$ rather than $\hat{\boldsymbol{\varepsilon}}$. This can be avoided by rearranging the enriched strain definition in Eq. (42) as

$$\nabla^s \mathbf{u} = \mathbb{T}^{-1} : \hat{\boldsymbol{\varepsilon}} - \frac{1}{\alpha} \mathbb{T}^{-1} : \mathbf{I} (\hat{\varepsilon}^v - \mathbf{I} : \mathbb{T} : \nabla^s \mathbf{u}) \quad (45)$$

and substituting it into Eq. (44a).

We can now observe that with the proposed choice of ‘‘closest isotropic tensor’’ the equality

$$\hat{\kappa} := \frac{\mathbf{I} : \mathbb{T}^{-t} : \mathbb{C} : \mathbb{T}^{-1} : \mathbf{I}}{\alpha^2} = \frac{\mathbf{I} : \hat{\mathbb{C}} : \mathbf{I}}{\alpha^2} = \frac{\mathbf{I} : \mathbb{C} : \mathbf{I}}{\alpha^2} = \kappa$$

holds. This gives the final set of equations:

$$\int_{\Omega} \nabla^s \boldsymbol{\delta}_u : \boldsymbol{\sigma}(\boldsymbol{\varepsilon}) - \int_{\Omega} (\mathbf{I} : \mathbb{T} : \nabla^s \boldsymbol{\delta}_u) \hat{\kappa} (\hat{\varepsilon}^v - \mathbf{I} : \mathbb{T} : \nabla^s \mathbf{u}) = \int_{\Omega} \boldsymbol{\delta}_u \cdot \mathbf{f} \quad (46a)$$

$$- \int_{\Omega} \delta_{\hat{\varepsilon}^v} \hat{\kappa} (-\mathbf{I} : \mathbb{T} : \nabla^s \mathbf{u} + \hat{\varepsilon}^v) = 0 \quad (46b)$$

In essence, the mixed formulation that we propose for the anisotropic case consists in taking the displacement \mathbf{u} and the modified volumetric strain

$$\hat{\varepsilon}^v = \mathbf{I} : \mathbb{T} : \nabla^s \mathbf{u} = \text{Tr}(\mathbb{T} : \nabla^s \mathbf{u})$$

as unknowns instead of $\varepsilon^v = \text{Tr}(\nabla^s \mathbf{u}) = \nabla \cdot \mathbf{u}$.

3.3. Variational multi-scales stabilisation

The discussion needs to be completed by the definition of a suitable stabilisation. Proceeding similarly to the isotropic case, we can take a subgrid stabilisation in the form of (see Eqs. (17) with P_s being the identity):

$$\mathbf{u}_s = \tau_1 \left[\mathbf{f} + \nabla \cdot \left(\mathbb{C} : \nabla^s \mathbf{u}_h + \hat{\kappa} \left(\hat{\varepsilon}_h^v - \mathbf{I} : \mathbb{T} : \nabla^s \mathbf{u}_h \right) \mathbf{I} \right) \right] \quad (47a)$$

$$\hat{\varepsilon}_s^v = \tau_2 \left(\mathbf{I} : \mathbb{T} : \nabla^s \mathbf{u}_h - \hat{\varepsilon}_h^v \right) \quad (47b)$$

Upon substitution in the Galerkin form and assuming the use of linear FE, we obtain (see Eq. (20)):

$$\begin{aligned} & \int_{\Omega} \nabla^s \delta \mathbf{u}_h : \boldsymbol{\sigma}(\boldsymbol{\varepsilon}_h) + \int_{\Omega} (1 - \tau_2) \left(\mathbf{I} : \mathbb{T} : \nabla^s \delta \mathbf{u}_h \right) \hat{\kappa} \left(\hat{\varepsilon}_h^v - \mathbf{I} : \mathbb{T} : \nabla^s \mathbf{u}_h \right) \\ &= \int_{\Omega} \delta \mathbf{u}_h \cdot \mathbf{f} \end{aligned} \quad (48a)$$

$$\begin{aligned} & \int_{\Omega} (1 - \tau_2) \delta_{\hat{\varepsilon}_h^v} \hat{\kappa} \left(\hat{\varepsilon}_h^v - \mathbf{I} : \mathbb{T} : \nabla^s \mathbf{u}_h \right) \\ &+ \int_{\Omega} \tau_1 \hat{\kappa}^2 \nabla \delta_{\hat{\varepsilon}_h^v} \cdot \nabla \hat{\varepsilon}_h^v = - \int_{\Omega} \hat{\kappa} \nabla \delta_{\hat{\varepsilon}_h^v} \cdot \tau_1 \mathbf{f} \end{aligned} \quad (48b)$$

3.4. Finite element implementation — anisotropic case

As for the isotropic case, the residual in FE notation obtains slightly different forms depending on the choice of $\boldsymbol{\varepsilon}_h$. The option $\boldsymbol{\varepsilon}_h := \nabla^s \mathbf{u}_h - \frac{1}{\alpha} \nabla \cdot \mathbf{u}_h \mathbf{I} + \frac{1}{\alpha} \varepsilon_h^v \mathbf{I}$ gives

$$\mathbf{R}_I := \begin{pmatrix} N_I \mathbf{f}_{ext} - \mathbf{B}_I^t \boldsymbol{\sigma}(\boldsymbol{\varepsilon}_h) + \frac{1}{\alpha} \mathbf{B}_I^t \mathbf{C} \mathbf{T}^{-1} \mathbf{m} H_J - (1 - \tau_2) \hat{\kappa} \boldsymbol{\Psi}_I^t H_J \\ (1 - \tau_2) \hat{\kappa} N_I H_J + \hat{\kappa}^2 \mathbf{G}_I^t \tau_1 \mathbf{G}_J \varepsilon_{h,J}^v - \hat{\kappa} \mathbf{G}_I^t \tau_1 \mathbf{f} \end{pmatrix} \quad (49)$$

while the choice $\boldsymbol{\varepsilon}_h := \nabla^s \mathbf{u}_h$ results in

$$\mathbf{R}_I := \begin{pmatrix} N_I \mathbf{f}_{ext} - \mathbf{B}_I^t \boldsymbol{\sigma}(\boldsymbol{\varepsilon}_h) - (1 - \tau_2) \hat{\kappa} \boldsymbol{\Psi}_I^t H_J \\ (1 - \tau_2) \hat{\kappa} N_I H_J + \hat{\kappa}^2 \mathbf{G}_I^t \tau_1 \mathbf{G}_J \varepsilon_{h,J}^v - \hat{\kappa} \mathbf{G}_I^t \tau_1 \mathbf{f} \end{pmatrix} \quad (50)$$

with $\boldsymbol{\Psi}_J := \mathbf{m}^t \mathbf{T} \mathbf{B}_J$,

$$H_J := N_J \varepsilon_{h,J}^v - \boldsymbol{\Psi}_J^t \mathbf{u}_{h,J} \quad (51)$$

and

$$\hat{\kappa} := \frac{\mathbf{m}^t \mathbf{T}^{-t} \mathbf{C} \mathbf{T}^{-1} \mathbf{m}}{\alpha^2} \quad (52)$$

In either case, the LHS is identical and is given by

$$\begin{aligned} \text{LHS}_{IJ} := & \\ & \begin{pmatrix} \mathbf{B}_I^t \mathbf{C} \mathbf{B}_J - (1 - \tau_2) \hat{\kappa} \boldsymbol{\Psi}_I \boldsymbol{\Psi}_J^t & (1 - \tau_2) \hat{\kappa} \boldsymbol{\Psi}_I N_J \\ (1 - \tau_2) \hat{\kappa} N_I \boldsymbol{\Psi}_J^t & - (1 - \tau_2) \hat{\kappa} N_I N_J - \hat{\kappa}^2 \mathbf{G}_I^t \tau_1 \mathbf{G}_J \end{pmatrix} \end{aligned} \quad (53)$$

4. Results

4.1. Manufactured solution test

We begin the result section by verifying the convergence rates of the proposed formulation. To that end, we employ the Method of Manufactured Solutions [22] and focus on a problem defined over a unit square, positioned so that the bottom left corner coincides with the position (0,0). The chosen target displacement field is

$$\bar{\mathbf{u}} = A \begin{pmatrix} \sin(4\pi x) \\ \cos(4\pi y) \\ 0 \end{pmatrix}$$

Table 1

Incompressible isotropic material manufactured solution test. \mathbf{u} and ε^v strain error norms.

n	1	2	3	4	5	6	7	8	9
h	0.5	0.25	0.125	6.25e-2	3.13e-2	1.56e-2	7.81e-3	3.91e-3	1.95e-3
$\ \mathbf{u} - \bar{\mathbf{u}}\ _{L^2(\Omega)}$	2.56e-1	3.57e-2	1.38e-2	2.60e-3	5.66e-4	1.34e-5	3.26e-5	8.06e-6	2.00e-6
$\ \varepsilon^v - \varepsilon^v\ _{L^2(\Omega)}$	5.37e-2	1.95e-2	1.73e-3	5.37e-4	1.94e-4	6.56e-5	2.24e-5	7.79e-6	2.73e-6

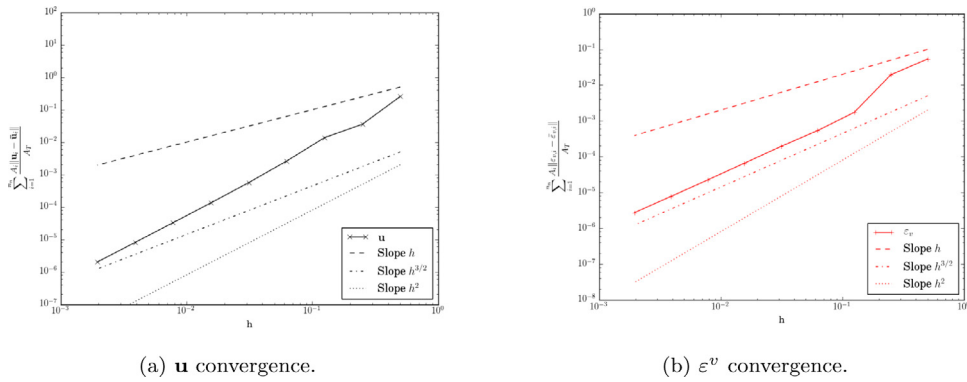


Fig. 1. Manufactured solution test. Incompressible isotropic material convergence analysis. τ_1 computed with \mathbb{C} .

where A represents an adjustable amplification factor which in our tests is set to 10^{-3} to ensure that the solution remains well within the small strain regime. Such displacement field yields the volumetric strain field

$$\varepsilon^v = 4\pi A (\cos(4\pi x) - \sin(4\pi y))$$

The force field in equilibrium with such displacement can be obtained by substitution into Eq. (2) to give

$$\bar{\mathbf{f}} = (4\pi)^2 A \begin{pmatrix} C_{00} \sin(4\pi x) + C_{21} \cos(4\pi y) \\ C_{11} \cos(4\pi y) + C_{20} \sin(4\pi x) \\ 0 \end{pmatrix}$$

where the coefficients C_{ij} are the entries of the Voigt form of the constitutive tensor. For the sake of the benchmark, the domain is meshed using a linear quadrilateral structured mesh with 2^n lateral subdivisions. Different choices of the elastic parameters are employed with the aim of evaluating the performance in different conditions.

4.1.1. Incompressible isotropic material

A plain strain constitutive law with the material properties E and ν equal to 200 N/m² and 0.4999 is used with the aim of assessing the convergence at the incompressible limit.

Table 1 collects the \mathbf{u} and ε^v error norms for each one of the meshes we use. These results are also depicted in Fig. 1. We observe that the convergence is quadratic for the \mathbf{u} field and $h^{3/2}$ for the ε^v field.

4.1.2. Anisotropic material

A plane-strain anisotropic material is checked next, using the constitutive tensor

$$\mathbb{C} = \begin{pmatrix} 54469.29 & 8284.82 & 17726.94 \\ 8284.82 & 5981.77 & 2615.99 \\ 17726.94 & 2615.99 & 8305.89 \end{pmatrix} \tag{54}$$

The calculated \mathbf{C}_{iso} and \mathbf{T} matrices are

$$\mathbf{C}_{iso} = \begin{pmatrix} 29692.637 & 8817.713 & 0. \\ 8817.713 & 29692.637 & 0. \\ 0. & 0. & 10437.462 \end{pmatrix} \tag{55}$$

Table 2
Anisotropic material manufactured solution test. \mathbf{u} and ε^v strain error norms.

n	1	2	3	4	5	6	7	8	9
h	0.5	0.25	0.125	6.25e-2	3.13e-2	1.56e-2	7.81e-3	3.91e-3	1.95e-3
$\ \mathbf{u} - \bar{\mathbf{u}}\ _{L^2(\Omega)}$	2.08e-2	1.94e-3	2.58e-3	1.33e-3	4.11e-4	1.09e-4	2.76e-5	6.92e-6	1.73e-6
$\ \hat{\varepsilon}^v - \varepsilon^v\ _{L^2(\Omega)}$	1.94e-2	1.61e-2	2.13e-2	9.89e-3	3.03e-3	8.05e-4	2.07e-4	5.36e-5	1.41e-5

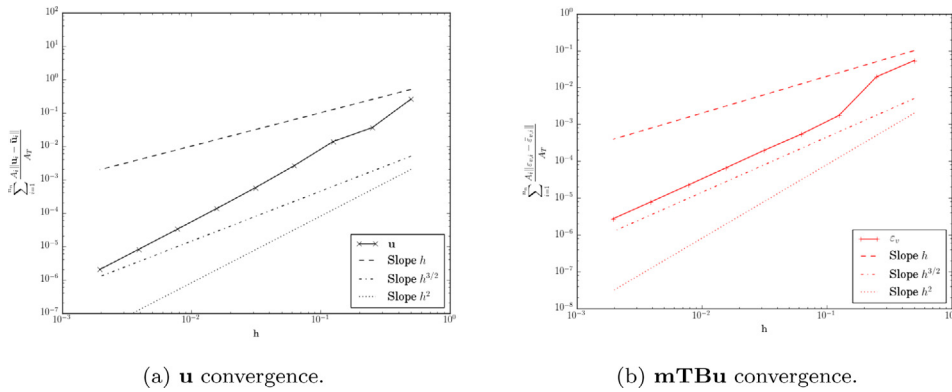


Fig. 2. Manufactured solution test. Anisotropic material convergence analysis. τ_1 computed with \mathbb{C} .

and

$$\mathbf{T} = \begin{pmatrix} 1.32161932 & 0.0931325 & 0.35389397 \\ -0.04531568 & 0.41023417 & -0.01086188 \\ 0.58737628 & 0.07153362 & 0.66756935 \end{pmatrix} \tag{56}$$

We recall that in the anisotropic case, the obtained “volumetric strain” is not any longer $\nabla \cdot \mathbf{u}$ but $\mathbf{I} : \mathbb{T} : \nabla^s \mathbf{u}_h$. After computing the anisotropy matrix \mathbb{T} corresponding to the constitutive matrix in Eq. (54), we obtain the analytical volumetric strain field $\bar{\varepsilon}^v = 4\pi A (1.2763 \cos(4\pi x) - 0.503367 \sin(4\pi y))$.

Table 2 collects the \mathbf{u} and $\hat{\varepsilon}^v$ error norms for each one of the meshes we use. These results are also depicted in Fig. 2.

4.2. 2D Cook’s membrane

The second benchmark test considered is the well known Cook’s membrane benchmark, described for example in [8]. The setup of the test is shown in Fig. 3. A vertical line load of 6.25×10^{-3} N/mm is applied at the right edge (amounting to a total load of 0.1 N). A plain strain constitutive model with unit thickness is used in all the 2D simulations. The proposed mixed formulation is tested with linear triangle and bilinear quadrilateral elements. The obtained results are compared with irreducible linear triangle and bilinear quadrilateral elements as well as with Bbar elements.

4.2.1. Incompressible isotropic material

We first conduct the test using a linear elastic plane strain constitutive law with the material properties stated in Fig. 3. The plot of the y-displacement on the top right point is shown in Fig. 4 for uniform mesh subdivisions by factors 2-2⁹. We observe that the proposed formulation converges much faster to the expected value than the irreducible one. When comparing to the Q1P0 (Bbar) element, the proposed formulation exhibits a slightly better behaviour for the coarser meshes.

Complementarily, we solve the problem for a set of unstructured triangular meshes whose sizes can be computed as $5/2^n$, $n \in (0, 6)$. Fig. 5 depicts the y-displacement convergence on the top right point. The superior performance of the mixed \mathbf{u} - ε^v formulation becomes evident in this case.

Finally, we also present a view of selected results in Fig. 6 which shows that a good solution is found for all the variables of interest.

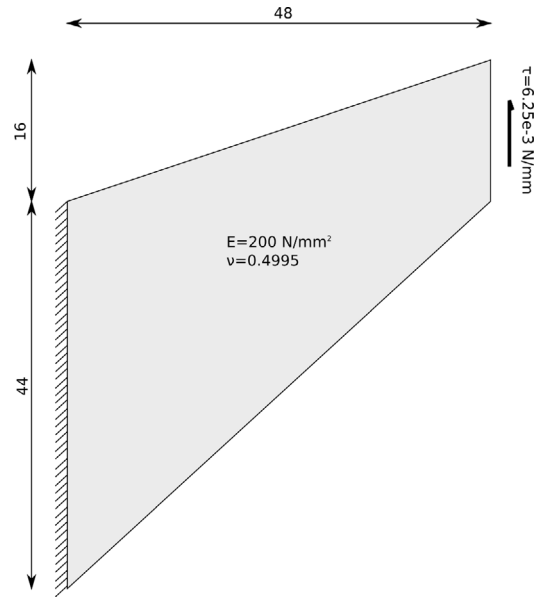


Fig. 3. Setup of Cook's Membrane Benchmark [mm].

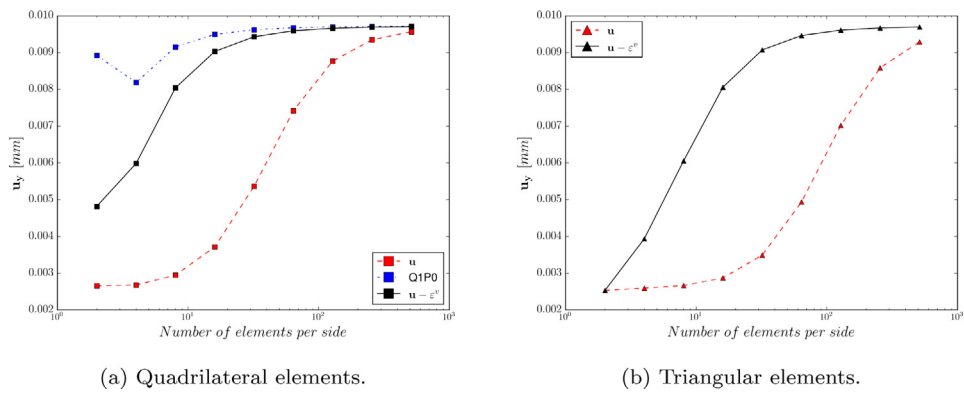


Fig. 4. Cook's membrane test. Incompressible isotropic material u_y structured meshes convergence results.

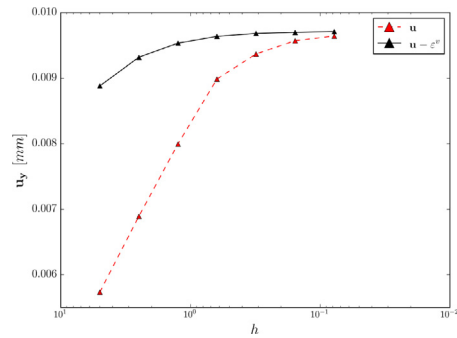


Fig. 5. Cook's membrane test. Incompressible isotropic material u_y unstructured triangular mesh convergence results.

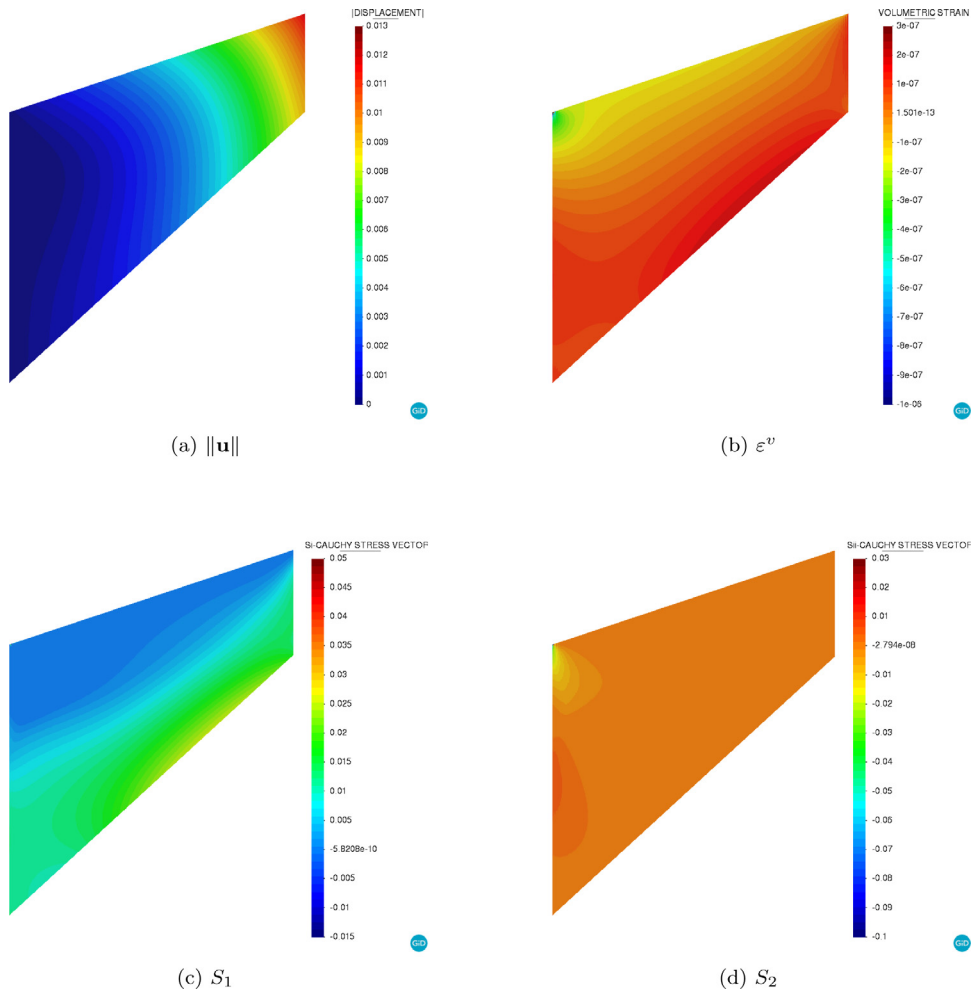


Fig. 6. Cook's membrane test. Solution snapshots for the 256 divisions quadrilateral mesh (S_1 , S_2 : principal stresses).

4.2.2. Incompressible anisotropic material

We carry out the same test but using an incompressible anisotropic material whose response is modelled by the constitutive tensor

$$\mathbb{C} = \begin{pmatrix} 970870.07 & 1239555.39 & 0.0 \\ 1239555.39 & 1622077.42 & 0.0 \\ 0.0 & 0.0 & 6711.41 \end{pmatrix}$$

with the associated \mathbb{C}_{iso} and \mathbf{T} matrices

$$\mathbb{C}_{iso} = \begin{pmatrix} 1292124.1915 & 1243904.9435 & 0. \\ 1243904.9435 & 1292124.1915 & 0. \\ 0. & 0. & 24109.624 \end{pmatrix} \tag{57}$$

and

$$\mathbf{T} = \begin{pmatrix} 0.34121548 & -0.20655167 & 0. \\ 0.53340404 & 1.31787552 & 0. \\ 0. & 0. & 0.52760836 \end{pmatrix} \tag{58}$$

Fig. 7 presents the convergence results. Once again, the proposed mixed formulation far outperforms the irreducible approach.

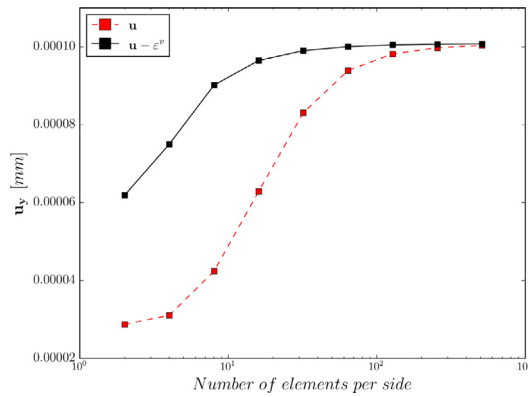


Fig. 7. Cook’s membrane test. Incompressible anisotropic material u_y convergence results.

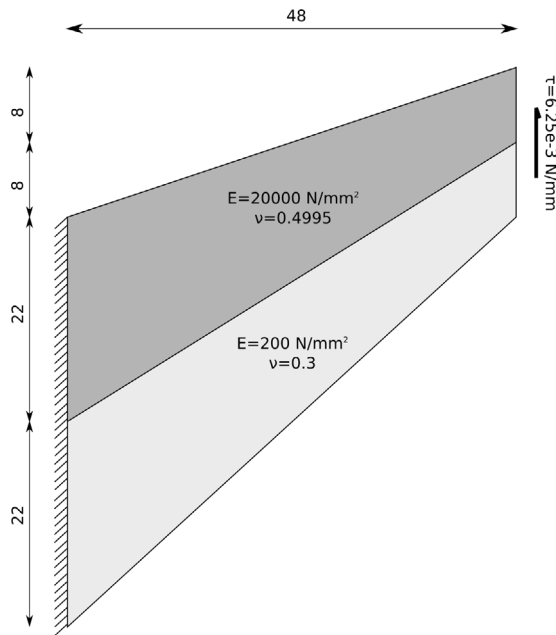


Fig. 8. Setup of Cook’s Membrane Benchmark using two distinct materials [mm].

4.3. 2D bimaterial Cook’s membrane

4.3.1. Two isotropic materials

In the third test, we modify the second benchmark by introducing two different materials as shown in Fig. 8. Only one of the two materials is considered incompressible in order to introduce a large difference in the constitutive behaviour. Thus, $E = 2.0 \times 10^4$ Pa and $\nu = 0.4995$ in the top half of the membrane while $E = 2.0 \times 10^2$ Pa and $\nu = 0.3$ in the bottom half.

We shall remark that introducing a discontinuity in the material is classically challenging for mixed approaches, but the proposed approach seems to handle the case without difficulties, thus proving that one of the design goals of the method is accomplished.

The plot of vertical displacement vs. mesh subdivision for such configuration is shown in Fig. 9.

Fig. 10 shows a view of the u , ϵ^v and stress fields showing that no spurious oscillations are found.

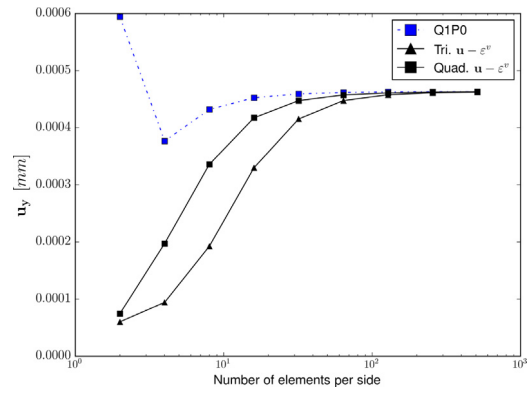


Fig. 9. Bimaterial Cook’s membrane test. u_y convergence.

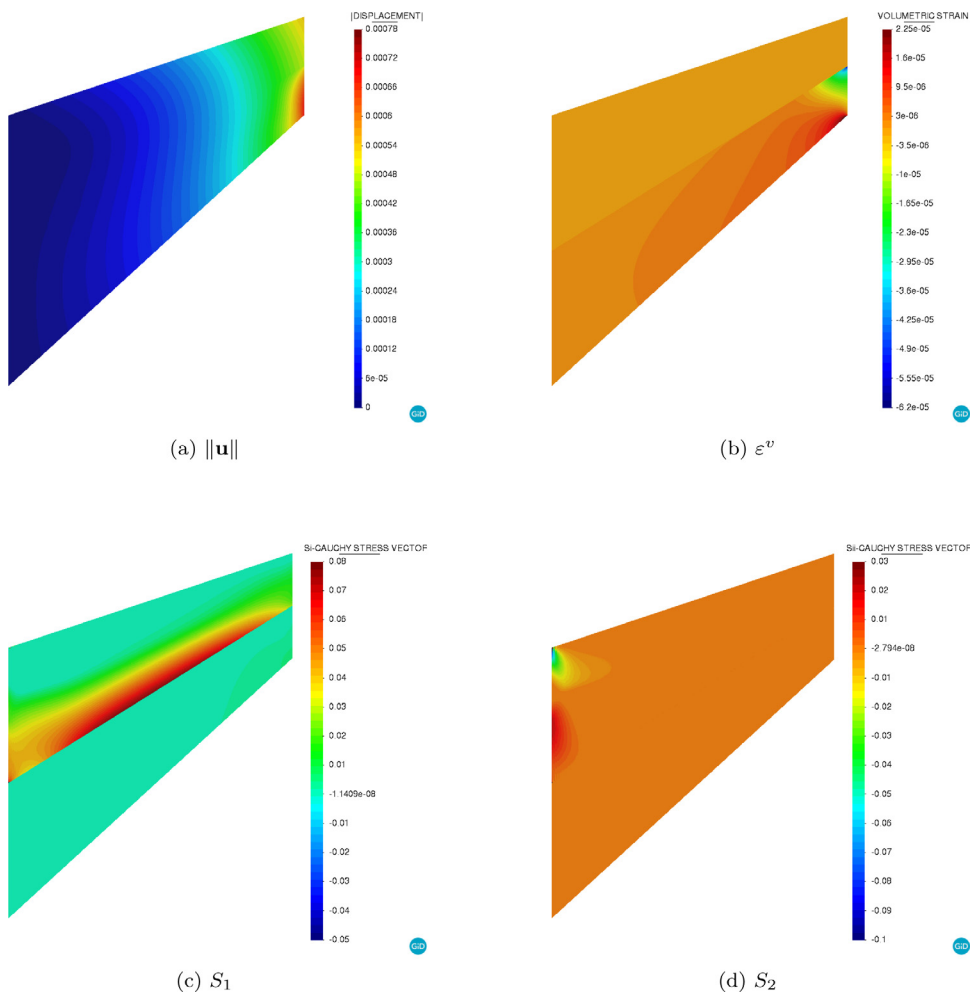


Fig. 10. Bimaterial Cook’s membrane test. Solution snapshots for the 256 divisions quadrilateral mesh.

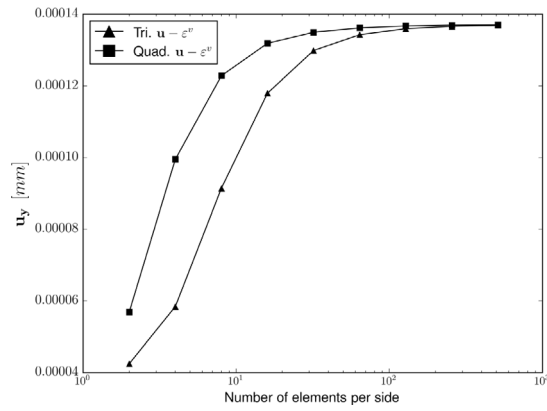


Fig. 11. Bimaterial (isotropic–anisotropic) Cook’s membrane test. u_y convergence.

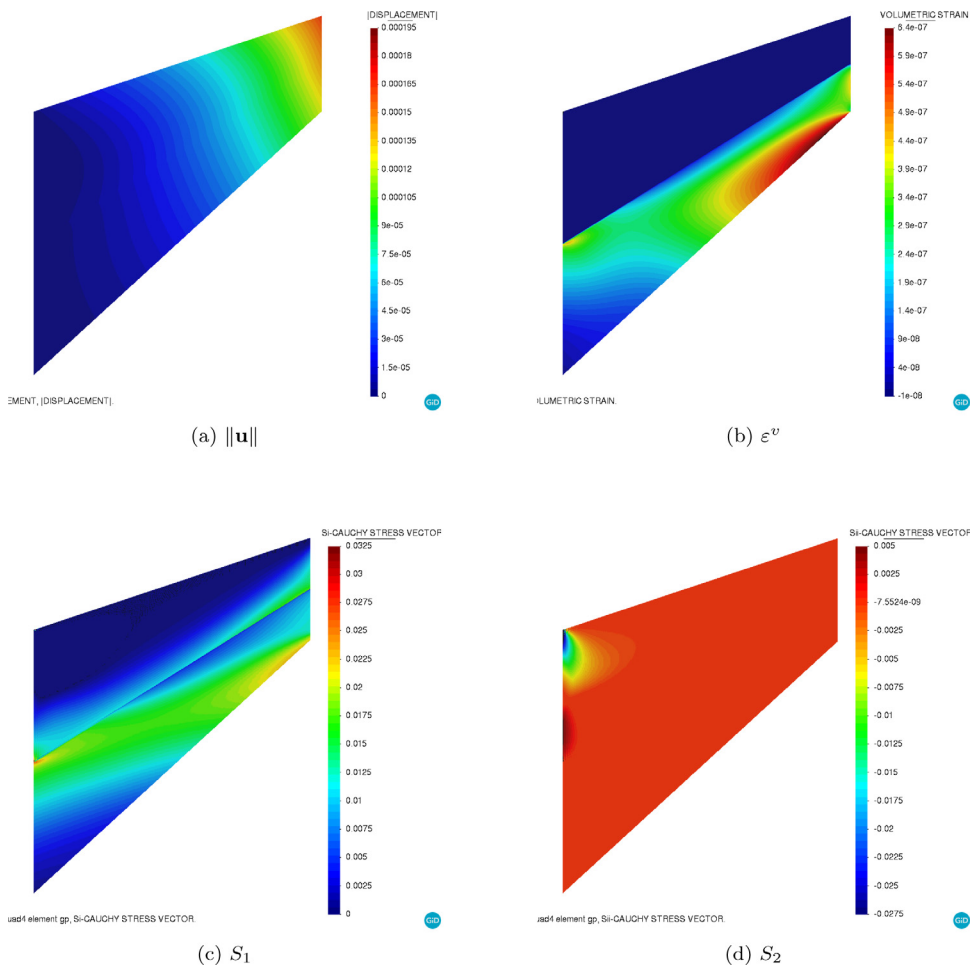


Fig. 12. Bimaterial (isotropic–anisotropic) Cook’s membrane test. Solution snapshots for the 256 divisions quadrilateral mesh.

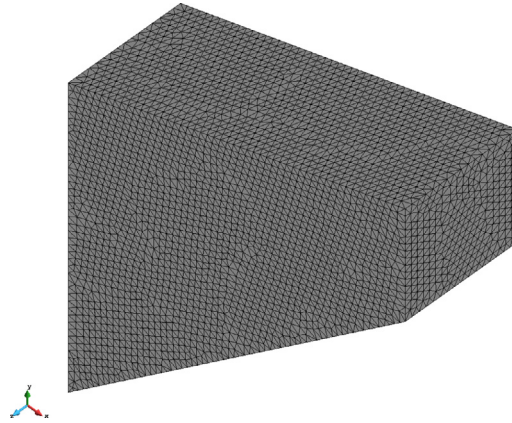


Fig. 13. 3D anisotropic Cook's membrane. Unstructured linear tetrahedra mesh.

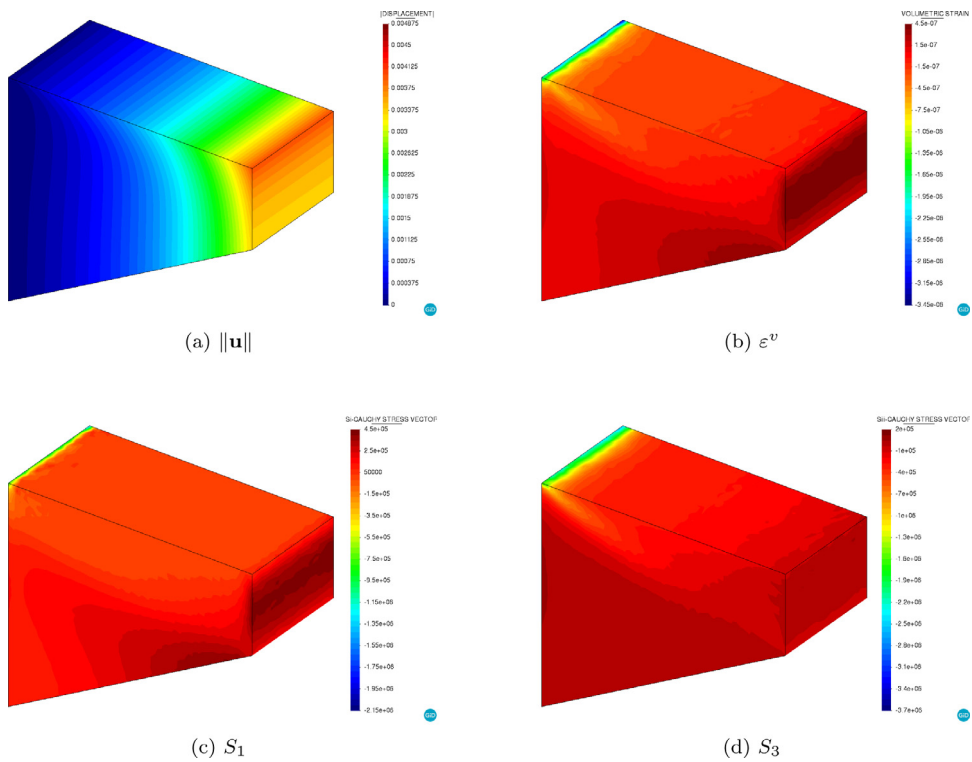


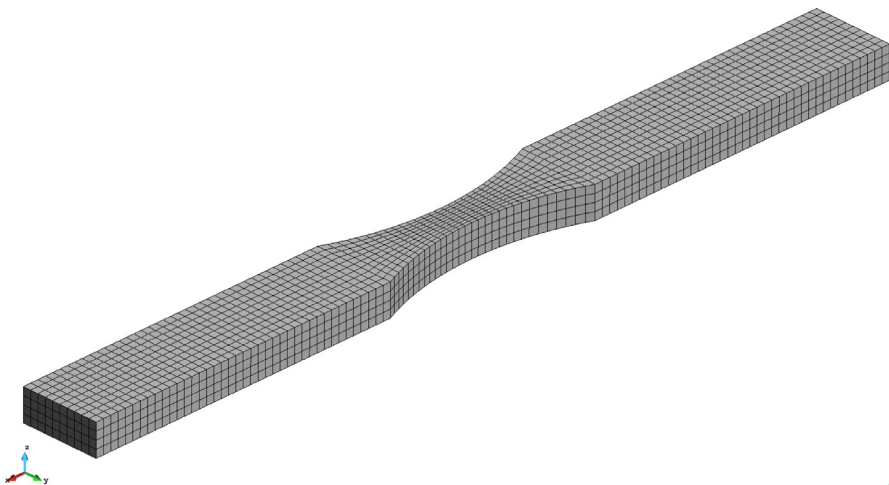
Fig. 14. 3D anisotropic Cook's membrane. Solution snapshots.

4.3.2. Isotropic–anisotropic materials

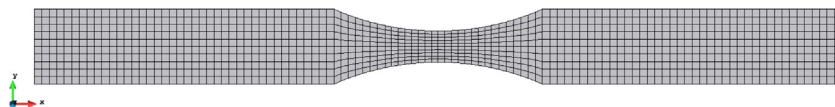
We repeat the same bimaterial Cook's membrane example but substituting the isotropic material in the bottom half of the membrane by the anisotropic one characterised by the constitutive tensor

$$C = \begin{pmatrix} 54469.29 & 8284.82 & 17726.94 \\ 8284.82 & 5981.77 & 2615.99 \\ 17726.94 & 2615.99 & 8305.89 \end{pmatrix}$$

The plot of vertical displacement vs. mesh subdivision for such configuration is shown in Fig. 11. Fig. 12 shows a view of the \mathbf{u} , ε^v and stress fields showing that no spurious oscillations are found.

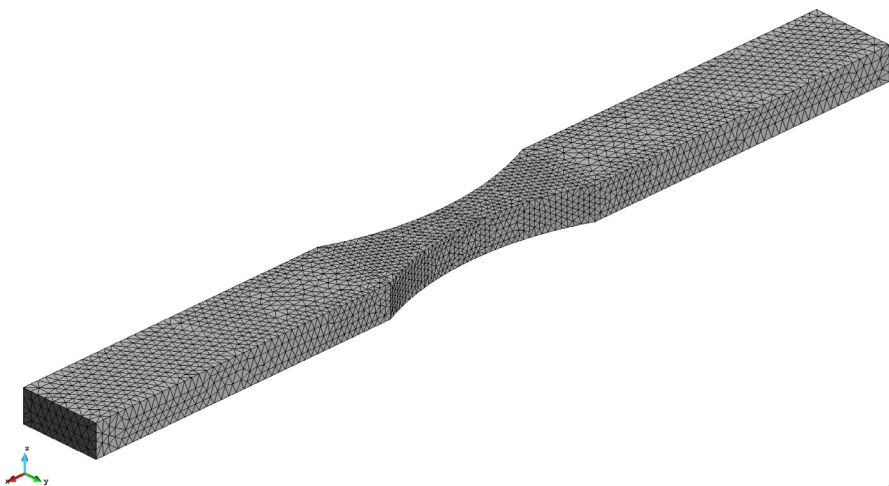


(a) Isometric view.



(b) xy -plane view.

Fig. 15. 3D necking bar. Structured hexahedra mesh.



(a) Isometric view.



(b) xy -plane view.

Fig. 16. 3D necking bar. Structured tetrahedra mesh.

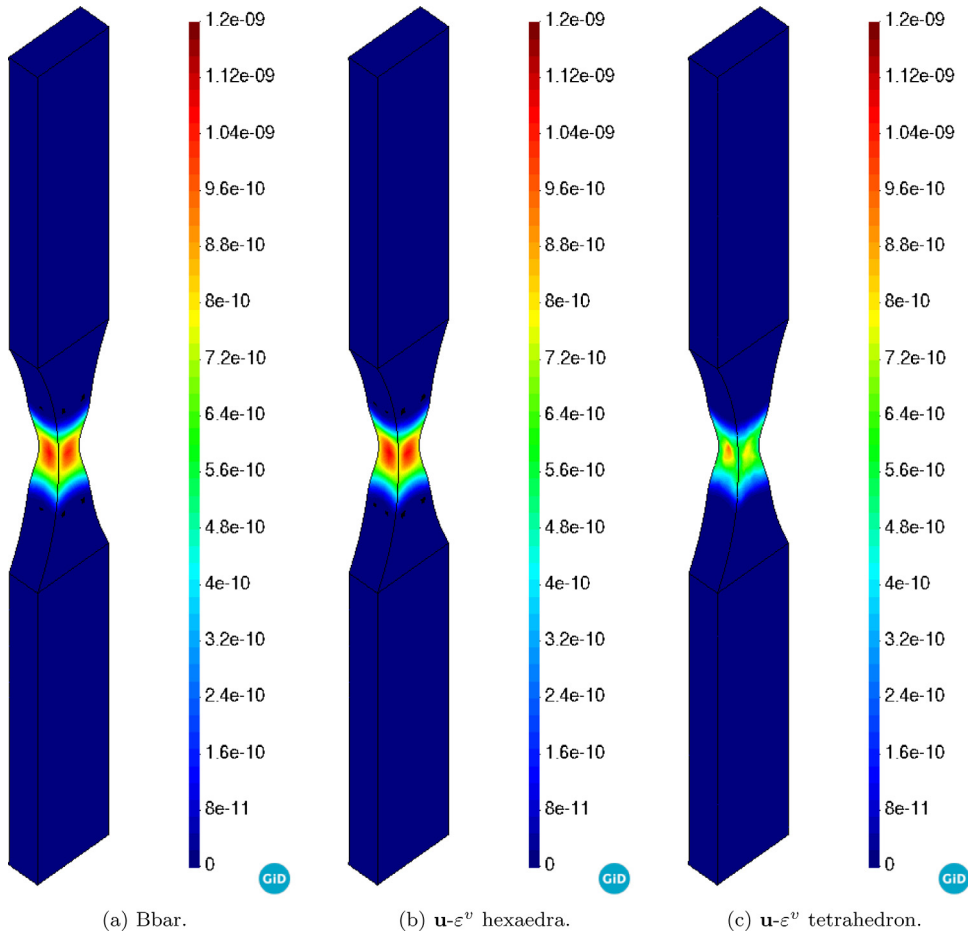


Fig. 17. 3D necking bar. Plastic dissipation (deformation scale x 40).

4.4. 3D anisotropic Cook's membrane

We extrude the same geometry by 16 mm. The surface load is now 10^5 N/mm^2 , corresponding to a total load of $25.6 \times 10^6 \text{ N}$. We fix the out of plane displacements on the front and rear surfaces. The anisotropic constitutive tensor we use is

$$\mathbf{C}_{aniso} := \begin{pmatrix} 5.99E+11 & 5.57E+11 & 5.34E+11 & 0 & 0 & 4.44E+09 \\ 5.57E+11 & 5.71E+11 & 5.34E+11 & 0 & 0 & -3.00E+09 \\ 5.34E+11 & 5.34E+11 & 5.37E+11 & 0 & 0 & 9.90E+05 \\ 0 & 0 & 0 & 1.92E+09 & 9.78E+06 & 0 \\ 0 & 0 & 0 & 9.78E+06 & 2.12E+09 & 0 \\ 4.44E+09 & -3.00E+09 & 9.90E+05 & 0 & 0 & 2.56E+10 \end{pmatrix} \quad (59)$$

We use an unstructured mesh conformed by around 230k linear tetrahedral elements (Fig. 13).

As can be seen in Fig. 14, smooth results are obtained for all the fields thus confirming that the formulation also works correctly in the 3D case.

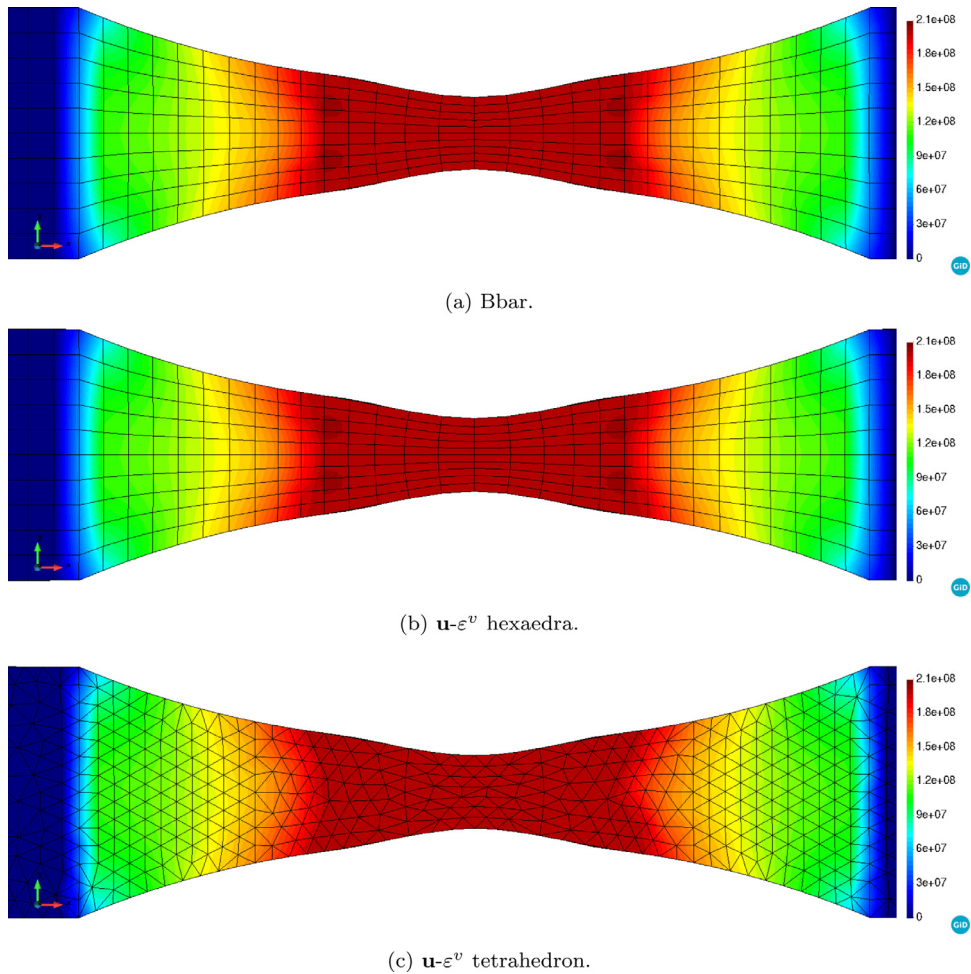


Fig. 18. 3D necking bar. Uniaxial stress [Pa] (deformation scale x40).

4.5. 3D necking bar

The objective of the benchmark is to compare the behaviour of the proposed formulation, using both a structured and unstructured discretisation, to a reference Bbar implementation in a case involving plasticity. To that purpose we solve the well-known necking bar example using a perfect isotropic J2 plasticity law. The Young modulus, Poisson ratio, and yield stress are 210×10^9 GPa, 0.29 and 200 MPa respectively. The specimen, whose dimensions are $5.4 \times 0.5 \times 0.2$ cm³, is clamped at its left face while an incremental total displacement of 0.006 cm is imposed at its right face.

A structured hexahedral mesh conformed by 4.4k elements (Fig. 15) is employed. A fairly similar discretisation level in terms of element sizes is achieved with an unstructured mesh of around 33k tetrahedra (Fig. 16).

Figs. 17 and 18 present the plastic dissipation and the uniaxial stress obtained for the three cases. As it can be observed in Fig. 18 the final deformed shape and the uniaxial stress distribution is very similar in all the cases. No spurious oscillations are visible in the mixed solution. Plastic dissipation is slightly underestimated in the unstructured mesh results, probably because of a slightly stiffer behaviour of the tetrahedral element.

4.6. Automotive machinery piece

This last example presents the (purely qualitative) results of a simulation involving the plastic deformation of an industrial piece. The problem consists in the mechanical analysis of an aluminium object from the

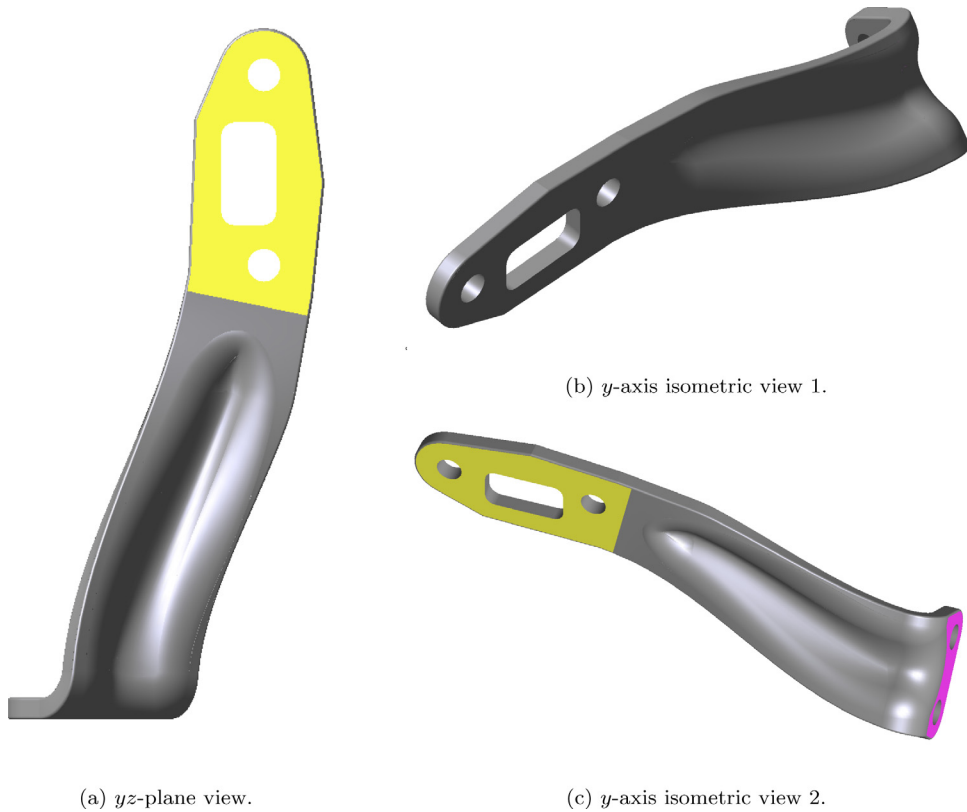


Fig. 19. Automotive machinery piece. Problem geometry. (For interpretation of the references to colour in this figure legend, the reader is referred to the web version of this article.)

automotive industry. The testcase is selected to showcase the capability of the method in application to a realistic usecase involving both elastic and inelastic regions, in which a standard tetrahedral formulation would perform unsatisfactorily.

The specimen (Fig. 19) has a length around 280 mm and a thickness of 8.5 mm. It is clamped in the magenta region in Fig. 19c. A surface load of 300 kPa is incrementally applied in the yellow region in Fig. 19c.

The material response is modelled using an isotropic small strain perfect J2 plasticity law. E and ν are set to 70 GPa and 0.35. The plastic regime is characterised by the yield stress $\sigma_y = 120$ MPa. Such material model implies a quasi-incompressible behaviour within the plastic region (implying that the volumetric deformation will be small compared to the total deformation), thus making unappealing the use of low order irreducible elements. The complexity of the shape prevents the use of Bbar type hexahedral meshes, thus leaving the proposed $\mathbf{u}-\varepsilon^v$ technology as one of the few possible alternatives.

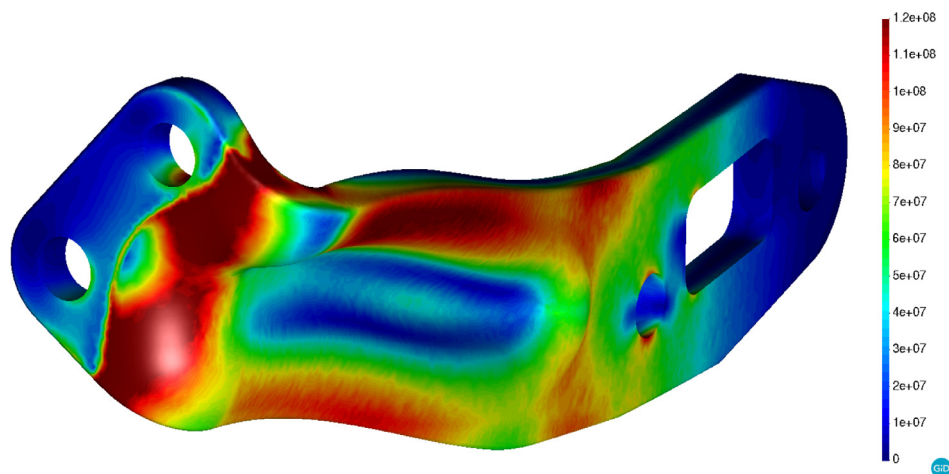
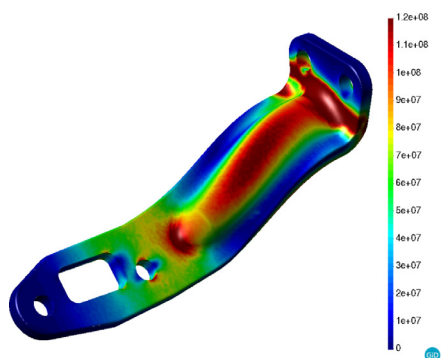
The domain was meshed using 550k linear tetrahedra, employing the proposed mixed formulation.

Fig. 20 depicts the obtained results. The piece shows a rather ductile behaviour up to the point at which a plastic hinge appears in the vicinity of the clamping (Fig. 20c).

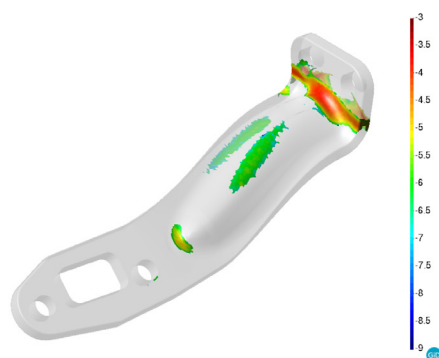
Fig. 20 collects a set of snapshots describing the evolution of the plastic deformation. More specifically, it can be noted that prior to the formation of the plastic hinge at the basis, large parts of the specimen reach the yield stress (120 MPa) (Figs. 20a and 20b) and thus present a plastic energy dissipation (Fig. 20c).

5. Conclusion

The paper presents a novel mixed element, which is able to tackle the quasi-incompressible limit. The proposed formulation aims at addressing problems with material nonlinearity, and is effective also in the presence of multiple material interfaces. A convenient modification that allows dealing with initially anisotropic problems is described. The proposed mixed method is also proved effective in combination with a plastic material behaviour.

(a) Uniaxial stress rear view [Pa] (deformation scale $\times 5$).

(b) Uniaxial stress lateral view [Pa].



(c) Plastic dissipation (log scale).

Fig. 20. Automotive machinery piece. Plasticity magnitudes isometric view.

Declaration of competing interest

The authors declare that they have no known competing financial interests or personal relationships that could have appeared to influence the work reported in this paper.

Acknowledgments

This research has been partly supported by the European Commission (EC) through the project ExaQUte (H2020-FETHPC-2016-2017-800898). The authors also acknowledge financial support from the Spanish Ministry of Economy and Competitiveness, through the “Severo Ochoa Programme for Centres of Excellence in R& D” (CEX2018-000797-S). R. Codina acknowledges the support received from the ICREA Acadèmia Research Program, from the Catalan Government.

References

- [1] E.A.S. Neto, F.M.A. Pires, D.R.J. Owen, F-bar-based linear triangles and tetrahedra for finite strain analysis of nearly incompressible solids. Part I: formulation and benchmarking, *Int. J. Numer. Methods Eng.* 62 (3) (2005) 353–383, <http://dx.doi.org/10.1002/nme.1187>.
- [2] Jaehyung Kim, Klaus-Jürgen Bathe, The finite element method enriched by interpolation covers, *Comput. Struct.* 116 (2013) 35–49, <http://dx.doi.org/10.1016/j.compstruc.2012.10.001>.
- [3] Robert L. Taylor, A mixed-enhanced formulation tetrahedral finite elements, *Int. J. Numer. Methods Eng.* 47 (1-3) (2000) 205–227, [http://dx.doi.org/10.1002/\(SICI\)1097-0207\(20000110/30\)47:1/3<255::AID-NME770>3.0.CO;2-0](http://dx.doi.org/10.1002/(SICI)1097-0207(20000110/30)47:1/3<255::AID-NME770>3.0.CO;2-0).

- [4] M. Chiumenti, Q. Valverde, C.A. de Saracibar, M. Cervera, A stabilized formulation for incompressible elasticity using linear displacement and pressure interpolations, *Comput. Methods Appl. Mech. Engrg.* 191 (2002) 5253–5264, [http://dx.doi.org/10.1016/S0045-7825\(02\)00443-7](http://dx.doi.org/10.1016/S0045-7825(02)00443-7).
- [5] M. de Mier Torrecilla, *Numerical Simulation of Multi-Fluid Flows with the Particle Finite Element Method*, (Ph.D. thesis), Universitat Politècnica de Catalunya. Departament de Resistència de Materials i Estructures a l'Enginyeria, 2010.
- [6] N. Abboud, G. Scovazzi, Elastoplasticity with linear tetrahedral elements: A variational multiscale method, *Internat. J. Numer. Methods Engrg.* 115 (2018) 913–955, <http://dx.doi.org/10.1002/nme.5831>.
- [7] M. Cervera, M. Chiumenti, R. Codina, Mixed stabilized finite element methods in nonlinear solid mechanics: Part i: Formulation, *Comput. Methods Appl. Mech. Engrg.* 199 (2010) 2559–2570, <http://dx.doi.org/10.1016/j.cma.2010.04.006>.
- [8] M. Chiumenti, M. Cervera, R. Codina, A mixed three-field fe formulation for stress accurate analysis including the incompressible limit, *Comput. Methods Appl. Mech. Engrg.* 283 (2015) 1095–1116, <http://dx.doi.org/10.1016/j.cma.2014.08.004>.
- [9] P. Dadvand, R. Rossi, E. Oñate, An object-oriented environment for developing finite element codes for multi-disciplinary applications, *Arch. Comput. Methods Eng.* 17 (2010) 253–297, <http://dx.doi.org/10.1007/s11831-010-9045-2>.
- [10] P. Dadvand, R. Rossi, M. Gil, X. Martorell, J. Cotela, E. Juanpere, S. Idelsohn, E. Oñate, Migration of a generic multi-physics framework to hpc environments, *Comput. & Fluids* 80 (2013) 301–309, <http://dx.doi.org/10.1016/j.compfluid.2012.02.004>.
- [11] N. Lafontaine, R. Rossi, M. Cervera, M. Chiumenti, Explicit mixed strain–displacement finite element for dynamic geometrically non-linear solid mechanics, *Comput. Mech.* 55 (2015) 543–559, <http://dx.doi.org/10.1007/s00466-015-1121-x>.
- [12] M. Cervera, N. Lafontaine, R. Rossi, M. Chiumenti, Explicit mixed strain–displacement finite elements for compressible and quasi-incompressible elasticity and plasticity, *Comput. Mech.* 58 (2016) 511–532, <http://dx.doi.org/10.1007/s00466-016-1305-z>.
- [13] M. Destrade, P. Martin, T. Ting, The incompressible limit in linear anisotropic elasticity, with applications to surface waves and elastostatics, *J. Mech. Phys. Solids* 50 (2002) 1453–1468, [http://dx.doi.org/10.1016/S0022-5096\(01\)00121-1](http://dx.doi.org/10.1016/S0022-5096(01)00121-1).
- [14] S. Federico, A. Grillo, S. Imatani, The linear elasticity tensor of incompressible materials, *Math. Mech. Solids* 20 (2015) <http://dx.doi.org/10.1177/1081286514550576>.
- [15] T.J. Hughes, G.R. Feijóo, L. Mazzei, J.-B. Quincy, The variational multiscale method—a paradigm for computational mechanics, *Comput. Methods Appl. Mech. Engrg.* 166 (1998) 3–24, [http://dx.doi.org/10.1016/S0045-7825\(98\)00079-6](http://dx.doi.org/10.1016/S0045-7825(98)00079-6), advances in Stabilized Methods in Computational Mechanics.
- [16] R. Codina, S. Badia, J. Baiges, J. Principe, Variational multiscale methods in computational fluid dynamics, in: E. Stein, R. Borst, T.J.R. Hughes (Eds.), *Encyclopedia of Computational Mechanics*, John Wiley & Sons Ltd., 2017, pp. 1–28, <http://dx.doi.org/10.1002/9781119176817.ecm2117>.
- [17] R. Codina, J. Principe, J. Baiges, Subscales on the element boundaries in the variational two-scale finite element method, *Comput. Methods Appl. Mech. Engrg.* 198 (2009) 838–852.
- [18] R. Codina, Stabilization of incompressibility and convection through orthogonal sub-scales in finite element methods, *Comput. Methods Appl. Mech. Engrg.* 190 (2000) 1579–1599.
- [19] R. Codina, Analysis of a stabilized finite element approximation of the oseen equations using orthogonal subscales, *Appl. Numer. Math.* 58 (2008) 264–283.
- [20] J. Baiges, R. Codina, Variational multiscale error estimators for solid mechanics adaptive simulations: An orthogonal subgrid scale approach, *Comput. Methods Appl. Mech. Engrg.* 325 (2017) 37–55, <http://dx.doi.org/10.1016/j.cma.2017.07.008>.
- [21] A. Norris, The isotropic material closest to a given anisotropic material, *J. Mech Mater. Struct.* 1 (2005) <http://dx.doi.org/10.2140/jomms.2006.1.223>.
- [22] P.J. Roache, Code verification by the method of manufactured solutions, *J. Fluids Eng.* 124 (2001) 4–10, <http://dx.doi.org/10.1115/1.1436090>.